Super-Strong Hydrogel Composites Reinforced with PBO Nanofibers for Cartilage Replacement

RESEARCH ARTICLE

Macromolecular Bioscience
www.mbs-journal.de

Super-Strong Hydrogel Composites Reinforced with PBO Nanofibers for Cartilage Replacement

Andreia S. Oliveira, João C. Silva, Mónica V. Loureiro, Ana C. Marques, Nicholas A. Kotov, Rogério Colaço, and Ana P. Serro*

Cartilage replacement materials exhibiting a set of demanding properties such as high water content, high mechanical stiffness, low friction, and excellent biocompatibility are quite difficult to achieve. Here, poly(*p*-phenylene-2,6-benzobisoxazole) (PBO) nanofibers are combined with polyvinyl alcohol (PVA) to form a super-strong structure with a performance that surpasses the vast majority of previously existing hydrogels. PVA–PBO composites with water contents in the 59–76% range exhibit tensile and compressive moduli reaching 20.3 and 4.5 MPa, respectively, and a coefficient of friction below 0.08. Further, they are biocompatible and support the viability of chondrocytes for 1 week, with significant improvements in cell adhesion, proliferation, and differentiation compared to PVA. The new composites can be safely sterilized by steam heat or gamma radiation without compromising their integrity and overall performance. In addition, they show potential to be used as local delivery platforms for anti-inflammatory drugs. These attractive features make PVA–PBO composites highly competitive engineered materials with remarkable potential for use in the design of load-bearing tissues. Complementary work has also revealed that these composites will be interesting alternatives in other industrial fields where high thermal and mechanical resistance are essential requirements, or which can take advantage of the pH responsiveness functionality.

1. Introduction

Articular cartilage is a highly organized connective tissue that contains a large volume of water molecules and few chondrocytes within an interwoven network composed of rigid collagen fibers and soft proteoglycans.[1] This hydrogel-like biological tissue exhibits a unique combination of properties such as high flexibility, mechanical strength and stiffness, ultralow friction, and excellent wear resistance that render it capable of responding to a wide variety of mechanical stimuli through conformational readjustments.[1,2] Unfortunately, due to its avascular nature and scarce cellular content, articular cartilage lesions have a limited ability to self-repair, often leading to osteoarthritis.[3–5] Depending on the severity of the damage, different strategies may be adopted to alleviate debilitating pain and restore mobility, delaying the need for a total joint replacement.[4] When pharmacological treatments and physiotherapy are no longer effective, cartilage restoration techniques can be applied, including

A. S. Oliveira, A. P. Serro
Centro de Química Estrutural
Institute of Molecular Sciences
and Department of Chemical Engineering
Instituto Superior Técnico
Universidade de Lisboa
Av. Rovisco Pais 1, Lisbon 1049-001, Portugal
E-mail: andreia.oliveira@tecnico.ulisboa.pt

A. S. Oliveira, A. P. Serro
Centro de Investigação Interdisciplinar Egas Moniz
Instituto Universitário Egas Moniz
Quinta da Granja, Monte de Caparica, Caparica 2829-511, Portugal

A. S. Oliveira, R. Colaço
Instituto de Engenharia Mecânica and Department of Mechanical Engineering
Instituto Superior Técnico
Universidade de Lisboa
Av. Rovisco Pais 1, Lisbon 1049-001, Portugal

J. C. Silva
Institute for Bioengineering and Biosciences and Department of Bioengineering
Instituto Superior Técnico
Universidade de Lisboa
Av. Rovisco Pais 1, Lisbon 1049-001, Portugal

J. C. Silva
Associate Laboratory i4HB–Institute for Health and Bioeconomy
Instituto Superior Técnico
Universidade de Lisboa
Av. Rovisco Pais 1, Lisbon 1049-001, Portugal

J. C. Silva
Centre for Rapid and Sustainable Product Development
Politécnico de Leiria
Rua de Portugal-Zona Industrial
Marinha Grande 2430-028, Portugal

The ORCID identification number(s) for the author(s) of this article can be found under https://doi.org/10.1002/mabi.202200240

DOI: 10.1002/mabi.202200240

microfracture, autologous chondrocyte implantation, and osteochondral autograft/allograft transplantation.[4,6–8] Despite some promising results, these clinical strategies entail long recovery periods (>1 year)[9] and have high failure rates (40% on average at <15 years)[3,6,7] especially in patients over 40 years of age.[4,6] It is therefore imperative to find new solutions that timely and properly repair the damaged cartilage to improve the patients' quality of life.

For several years now, researchers have been trying to develop materials with structures and properties similar to cartilage, but only a few have been able to demonstrate a comparable performance to that of this load-bearing soft tissue.[10–13] Hydrogels, three-dimensional polymeric networks capable to absorb and retain significant amounts of water or other fluids within their structure, have received considerable attention for this purpose.[14,15] Not only because they can mimic the swelling of natural cartilage tissue but also its tribological behavior, being expected to solve the problems of high friction rates associated with joint replacement prostheses by improving the lubrication mechanisms.[15,16] In addition, the viscoelastic nature of hydrogels facilitates the transfer of mechanical loads to adjacent tissues, preventing the accumulation of residual stresses at the implant-tissue interface.[17] To date, several polymeric hydrogels of natural and synthetic origin have been explored for the development of potential cartilage replacement or repair materials.[14,18] Among them, polyvinyl alcohol (PVA) has been widely used due to its many advantageous qualities.[19–23] The hydrogels made of PVA are easy to produce, stable at room temperature, inexpensive, have easily tunable properties, exceptional permeability and lubricity, and are highly biocompatible.[24–27] Cartiva SCI (Wright Medical Group NV, USA), a PVA-based implant developed to replace the big toe joint and commercialized in recent years, has evidenced benefits in terms of pain reduction and improved patient mobility.[28,29] However, as with other hydrogel materials, the weak mechanical resistance and limited durability of PVA has restricted its clinical application in the repair of large or severe cartilage defects in the major load-bearing joints of the human body.[10,30,31] Indeed, producing hydrogels that possess a high water content and mechanical strength/stiffness, emulating the behavior of the joint connective tissue, is extremely difficult and has rarely been accomplished,[10–13] because these properties are hard to conciliate.[11,32,33] Thus, creating new mimetic biomaterials with such combination of characteristics remains a great challenge.

Many studies are now focusing on overcoming these limitations by seeking reinforcement solutions that aim to properly restore these demanding soft tissues. Taking inspiration from the distinctive structure and composition of articular cartilage, special emphasis has been placed on adding strong, rigid components to soft polymer matrices. Among the most used stiff additives with promising results are carbon nanotubes,[34] nanofibers of natural and synthetic origin,[10,11,33,35–37] and a few ceramics.[38,39] The contrasting mechanical properties of the matrix and the reinforcement act synergistically to overcome the inferior mechanical performance of single-component hydrogel matrices.

High-performance fibers and nanofibers of carbon, aramid, and poly(*p*-phenylene-2,6-benzobisoxazole) (PBO) have been widely used in the production of composites with improved mechanical and thermal degradation properties for automotive, aerospace, military, and beyond, but few authors have explored their potential for biomedical applications.[40–43] Llorens-Gámez et al.[13] and Serafin et al.[44] demonstrated that reinforcing different hydrogels with carbon nanofibers significantly enhanced their mechanical properties turning them into good candidates for a wide range of advanced applications including in biomedicine and bioengineering. In turn, Xu et al.[11] developed hydrogel composites reinforced with aramid nanofibers with a very promising mechanical performance and adequate water contents, comparable to those of articular cartilage. Also, Guo et al.[45] were successful in fabricating aramid reinforced hydrogels with improved mechanical and antibacterial properties for wound dressings. Concerning PBO nanofibers, to the authors' knowledge, they have never been used in the reinforcement of hydrogel structures so far. PBO fibers are lightweight and exhibit excellent thermal stability, flame retardancy, creep resistance, and mechanical properties that far exceed those of aramid fibers (strength and modulus can be up to double in PBO).[40,46,47] Hu et al.[48] used PBO fibers to reinforce an epoxy resin-based dental material that showed significantly improved mechanical properties and a cell viability of more than 90% of mouse embryonic fibroblasts. Thus, the use of PBO for strengthening materials for biomedical applications seems to be a very promising route but still requiring further investigation.

Due to the high water absorption and retention capacity of hydrogels, they can be easily loaded with bioactive molecules and release them later in a controlled manner.[49,50] Therefore, the possibility of using these materials as platforms for the local drug delivery in cartilage repair/replacement systems has sparked an increasing interest. They allow achieving adequate levels of therapeutic agents in the target tissues, overcoming the limitations of other administration forms (e.g., adverse side effects or need for higher doses of drugs in systemic administration). In recent works it has already been demonstrated that PVA-based hydrogels can be used with prophylactic/therapeutic purposes for the vehiculation of nonsteroidal anti-inflammatory drugs (NSAIDs) useful to prevent/reduce inflammation and pain in the postoperative period.[27,51]

Another relevant issue in the production of cartilage substitutes is sterilization, a mandatory step to guarantee the biological safety of the implantable materials. Despite the known sensitivity of many hydrogels to conventional sterilization agents,[52] such as steam heat and gamma radiation, only a few researchers[53,54] have considered including the study of their effect on the material's properties. Yet, it is crucial that hydrogels withstand

M. V. Loureiro, A. C. Marques
Centro de Recursos Naturais e Ambiente
Instituto Superior Técnico
Universidade de Lisboa
Av. Rovisco Pais 1, Lisbon 1049-001, Portugal
N. A. Kotov
Biointerfaces Institute
Department of Chemical Engineering
and Department of Materials Science and Engineering
University of Michigan
Ann Arbor, MI 48109, USA

efficient sterilization in order to maintain adequate in vivo performance.

This study reports on the design of a new biomimetic composite that emulates the properties of articular cartilage. For the first time, PBO nanofibers produced from commercial Zylon fibers, were used as an efficient strengthening component in the synthesis of PVA hydrogels. Different concentrations of PBO were employed to obtain a suitable fibrous reinforcement. The produced materials were evaluated regarding chemical structure, thermal behavior, water content, swelling, and mechanical performance. The PVA–PBO composite that showed the closest resemblance to cartilage tissue was then sterilized using steam heat (autoclaving) or gamma radiation and its properties were reassessed and compared with those of the nonsterilized material. After choosing the most suitable sterilization method, the friction behavior, wear, and biocompatibility of the sterilized sample were investigated. Finally, diclofenac and ketorolac, two clinically approved anti-inflammatory drugs widely used after orthopedic surgeries,[55] were loaded individually into the elected material and in vitro drug release experiments were conducted.

2. Experimental Section

2.1. Samples Preparation

Nanofibers were obtained by treating PBO fibers with a mixture of trifluoroacetic acid (TFA, purity ≥99%, Sigma-Aldrich, St. Louis, MO, USA) and methanesulfonic acid (MSA, purity 99%, ACROS Organics, Thermo Fisher Scientific, Fair Lawn, NJ, USA), as reported elsewhere.[56] Predefined amounts of Zylon AS (as spun) chopped fibers (Toyobo Co. Ltd., Osaka, Japan) were added to a mixed solution of TFA:MSA (4:1 v/v) to acquire PBO nanofiber dispersions at different concentrations (0.2, 0.4, 0.6, 1, and 1.33% w/v). Simultaneously, a PVA (M_w 146–186 kDa, ≥99% hydrolyzed, Sigma-Aldrich) solution was prepared in pure TFA at 6% w/v. In all cases, complete dissolution took less than 24 h at room temperature (RT) under continuous magnetic stirring. The composites were produced by blending equal volumes of PVA and PBO solutions (20 mL each) in order to obtain several formulations with different PVA:PBO mass ratios (30:1, 15:1, 10:1, 6:1, and 4.5:1). Before mixing, the individual polymeric solutions were preheated in a water bath at 45 °C for 20 min. Once combined, the mixtures were shaken vigorously for about 15 s and immediately poured into Petri dishes (Ø80 mm). The glass plates were covered and thus left for 2 h to permit the release of air bubbles formed during blending. After that, the lids were lifted slightly (≈1 mm in high) and fixed for a further 2 h to accelerate the gelation process. Subsequently, the lids were removed, and the gels were left to age at RT for 20 h to ensure complete gelation. The resultant materials were then immersed in a large amount of pure water for 3 days, which was replaced every 8 h for solvent exchange. Finally, they were dried at 50 °C in an oven with forced air circulation for the first 24 h and then under high vacuum for another 24 h to maximize solvent removal. The composites obtained were designated as 30P1Z, 15P1Z, 10P1Z, 6P1Z, and 4.5P1Z, according to the mass ratios between the two components. PVA control samples (6% w/v, 20 mL) and PBO nanofiber films (1.33 % w/v, 20 mL) were also prepared under the same conditions, except that drying of the latter was only performed immediately prior to characterization to avoid the extensive aggregation of nanofibers. Before each characterization test and whenever required, the hydrogel materials were first rehydrated under the appropriate conditions at least 48 h in advance.

2.2. Samples Sterilization

Two different techniques were used to sterilize the materials: 1) steam heat (autoclaving) and 2) gamma radiation. In the first case, hydrogel samples were conditioned in closed tubes immersed in a specific volume of water or drug solution (0.05 mL mg^{-1} dry mass of material). Autoclaving was performed at 121 °C for 30 min in a UNICLAVE 88/75L vertical steam sterilizer (AJ Costa (Irmãos), Agualva-Cacém, Lisbon, Portugal). For the irradiation, the dried materials were packed and vacuum-sealed in polyamide/polyethylene bags (Penta Ibérica, Torres Vedras, Portugal). The samples were exposed to 25 kGy of gamma radiation obtained from a ^{60}Co source, at RT and with a dose of 5 kGy h^{-1}. Red 4304 dosimeters (Harwell Dosimeters, Didcot, Oxfordshire, UK) were used to confirm the absorbed dose.

2.3. Samples Characterization

2.3.1. Morphology

The morphology of the materials was assessed through scanning electron microscopy (SEM), using a field emission gun-scanning electron microscope (FEG-SEM, JSM-7001F, JEOL, Tokyo, Japan) operating at 5 kV. Cross-sections were prepared by brittle fracture of the samples in liquid nitrogen. Prior to observation, specimens were dehydrated by soaking in a series of ethanol solutions (purity ≥99.5%, José Manuel Gomes dos Santos Lda, Odivelas, Portugal) of increasing concentrations (70, 95, and 100% v/v) at RT followed by *t*-butyl alcohol (purity ≥99.5%, 2-methyl-2-propanol, PanReac AppliChem, Darmstadt, Germany) at 40 °C—each step was performed thrice and lasting 15 min.[57] The materials were then removed from the *t*-butyl alcohol, frozen in a refrigerator at 4 °C and placed in a low-vacuum oven for 24 h for complete sublimation of the solvent. Thereafter, they were coated with a thin layer of gold/palladium (Q150T ES sputter coater, Quorum Technologies, Lewes, UK).

2.3.2. Chemical Structure

Fourier transform infrared (FTIR) spectra of the materials were obtained using a Spectrum Two (PerkinElmer, Waltham, MA, USA) equipment with a PerkinElmer Universal Attenuated Total Reflectance (UATR) Two Accessory. Before FTIR readings, samples were placed in a vacuum oven at 37 °C for 48 h to remove any residual water. The spectra were acquired in the 4000–400 cm^{-1} range, with 4 cm^{-1} resolution, and by averaging 8 or 16 scans. For the analysis, all spectra were normalized.

2.3.3. Thermal Behavior

Differential scanning calorimetry (DSC) measurements were carried out on a 200 F3 Maia instrument (NETZSCH, Selb, Germany) in the temperature range of 20–260 °C at 10 °C min^{-1} and

with nitrogen as the purge gas (50 mL min^{-1}). Thermogravimetric analysis (TGA) was conducted on a STA7200 system (Hitachi, Ibaraki, Japan) from RT to 600 °C, with a heating rate of 10 °C min^{-1}, under a controlled nitrogen flow (100 mL min^{-1}). For both tests, samples (≈10 mg) were previously left under vacuum (48 h, 37 °C) and then sealed in aluminum crucibles. The melting temperature (T_m) was taken as the middle temperature of the fusion peak in the DSC thermograms, and the corresponding enthalpy of fusion (ΔH) was estimated from the total area of the T_m peak. For each material, at least three independent DSC or TGA scans were performed ($n \geq 3$).

2.3.4. Water Content and Swelling Capacity

Sample disks (Ø7 mm) hydrated in pure water were dried at 100 °C for 24 h. Their mass was measured, before and after the procedure, using an OHAUS Discovery DV215CD semi-micro balance (Ohaus Corporation, Parsippany, NJ, USA). The values obtained were used to estimate the water content (WC) and swelling capacity (SC) of the materials at equilibrium through the following equations:[19]

$$\mathrm{WC}\,(\%) = \frac{m - m_0}{m} \times 100 \quad (1)$$

$$\mathrm{SC}\,(\%) = \frac{m - m_0}{m_0} \times 100 \quad (2)$$

where m and m_0 denote the mass of the swollen and dry specimens, respectively. At least four samples of each type were used in the measurements ($n \geq 4$).

2.3.5. Mechanical Properties

The mechanical responses of the materials under tensile and compressive loads were accessed with a TA.XT Express Texture Analyzer (Stable Micro Systems, Godalming, Surrey, UK) equipped with a 50 N load cell. Uniaxial tensile tests were conducted at RT (≈25 °C) on water-swollen hydrogels. For such, dumbbell-shaped specimens (2.5 mm width and 10 mm gauge length) were clamped by the ends and stretched until failure at a strain rate of 0.5 mm s^{-1}. In addition, the tensile behavior of dried specimens with the aforementioned dimensions was also evaluated at a crosshead speed of 0.1 mm s^{-1} using an Instron 5566 Universal Testing machine (Instron Corporation, Norwood, MA, USA) with a 500 N load cell. Unconfined compression tests were carried out in water at 37 °C. A 0.5 N preload was applied before each compression to obtain reliable data. Sample disks (Ø8 mm), pre-equilibrated in the testing conditions (medium and temperature), were compressed by an upper moveable Ø20 mm plate at a speed of 0.1 mm s^{-1} to the maximum capacity of the force sensor. The unloading was performed at the same velocity, and the entire cycle was monitored. Cyclic compression tests were also conducted under the same conditions, using 100 consecutive cycles and up to a maximum strain of 30%. Tensile and compressive tangent moduli were calculated as the ratio of stress (σ) to strain (ε). The tensile toughness was considered as the total area under the σ–ε curve. The energy dissipated upon compression was determined by subtracting the area under the unloading curve from the total area below the loading curve. For each experimental group, all tests were performed at least five times ($n \geq 5$).

2.3.6. Tribological Behavior

The tribological testing of the materials was carried out on a ball-on-plate TRB^3 tribometer (Anton Paar, Graz, Austria). The friction measurements were performed in linear reciprocal mode with stationary 316L stainless-steel balls (Ø6 mm, surface roughness ≤0.1 µm, Luis Aparicio SL, Barcelona, Spain) on sliding flat specimens (30 mm length × 20 mm width × 2 mm height). Tests were conducted at RT (≈25 °C) using as lubricant phosphate buffered saline (PBS, Sigma-Aldrich). The samples, unsterilized or previously sterilized in water by autoclaving (see Section 4.2) were first dried (37 °C, high vacuum, 1 week), weighed, and then soaked for 48 h in the lubricating medium before starting the experiments. Normal loads ranging from 5 to 30 N were applied, and the sliding speed, stroke length, and total sliding distance were kept constant at 25 mm s^{-1}, 8 mm, and 12 m, respectively. The friction coefficient was calculated as the ratio between the frictional resistance force and the applied normal contact force. The average dynamic friction coefficient was determined from three runs ($n = 3$) on each material and excluding the initial and final 25% of the sliding path. After each test, the samples were washed thoroughly with pure water for 3 days to remove the PBS salts. The materials were then dried at 37 °C under high vacuum for a week and reweighed. Wear was determined as the percentual difference in the dry mass of the specimens before and after each test.[24]

2.3.7. In Vitro Cell Culture Studies

Cell Culture: Healthy human chondrocytes (Cell Applications Inc., San Diego, CA, USA) were obtained from nonpathologic articular cartilage. Cells were thawed and expanded in chondrocyte proliferation medium consisting of high-glucose Dulbecco's modified Eagle's medium (DMEM, Gibco, Thermo Fisher Scientific, Grand Island NY, USA) supplemented with 10% v/v fetal bovine serum (FBS, Gibco, Thermo Fisher Scientific), 1× MEM nonessential amino acid solution (100×, Sigma-Aldrich), 0.2 × 10^{-3} M L-Lascorbic acid (purity 99%, Sigma-Aldrich), 0.4 × 10^{-3} M L-proline (purity ≥99%, Sigma-Aldrich), and 1% v/v penicillin-streptomycin (Pen/Strep, Gibco, Thermo Fisher Scientific) at 37 °C in a humidified atmosphere of 5% CO_2. Cells were passaged to new flasks once 80–90% confluence was reached. The culture medium was fully renewed 2–3 times a week, and only cells from passages 3 to 5 were used in the studies.

Cytotoxicity: The cytocompatibility of the materials (Ø14 mm, 2 mm thick) was evaluated with human chondrocytes by MTT assay (indirect extract test) and direct contact test according to ISO 10993-5 guidelines.[58] Before in vitro testing, the samples were sterilized in water by autoclaving (see Section 4.2). For both tests, cells were seeded at 1.2 × 10^5 cells/well in 24-well tissue culture treated polystyrene plates and cultivated to confluence in chondrocyte proliferation medium for 24 h at 37 °C and 5% CO_2. Cells grown directly on the well plates were considered as

negative controls, while latex was used as a positive control for cytotoxicity. For the indirect assay, each sterile sample disk was incubated in culture medium (3 cm^2 mL^{-1}) for 24 h under the previously mentioned conditions. The chondrocytes were then exposed to the extracted medium containing the hydrogel leachout products for 48 h at 37 °C and 5% CO_2. Afterward, the conditioned medium was aspirated and the MTT assay was performed using an In Vitro Toxicology Assay Kit – MTT based (Sigma-Aldrich) following the manufacturer's guidelines. In brief, cells were incubated with an MTT (3-(4,5-dimethylthiazol-2-yl)-2,5-diphenyl tetrazolium bromide) solution at 1 mg mL^{-1} for 4 h at 37 °C. After carefully removing the MTT medium, the resulting formazan crystals were dissolved in acidified isopropanol (0.1 N hydrochloric acid) under agitation for 5 min. The spectrophotometric absorbance values of the purple solutions were measured in an Infinite M200 PRO microplate reader (TECAN, Männedorf, Switzerland) at 570 nm. The percentage of viable chondrocytes was calculated by comparison with the values obtained for the negative control cultures. Four sample replicates ($n = 4$) were tested per experimental condition, and for each one, the absorbance was read in triplicate. The cytotoxicity of the materials via the direct contact test was evaluated after placing the sterile disks on top of a confluent monolayer of cells for 48 h at 37 °C and 5% CO_2. The viability and morphology of chondrocytes were then qualitatively assessed using an inverted optical LEICA DMI3000B microscope (Leica Microsystems, Germany) coupled to a Nikon DXM1200F digital camera (Nikon Instruments Inc., Japan). A total of three replicates ($n = 3$) per condition were used, and in each, several representative areas were imaged.

Biocompatibility Assessment: *Cell Seeding and Culture on Samples*: Prior to cell culture studies, the materials (Ø10 mm, 2 mm thick) were sterilized in water by autoclaving (see Section 4.2), rinsed three times with PBS + 1% v/v Pen/Strep solution and incubated in culture medium for 1.5 h at 37 °C. Human chondrocytes were harvested and seeded onto the hydrogel materials at a density of 1.5×10^5 cells/sample and placed in an ultra-low attachment tissue culture plate. The hydrogel discs were then incubated for 2 h without culture medium to favor initial cell adhesion, and afterward 1 mL of chondrocyte proliferation medium was poured into each well. The cultures were kept for 7 days in an incubator at 37 °C and 5% CO_2, and the medium was completely renewed every 2–3 days.

Cell Proliferation Assay: Cell proliferation was assessed by evaluating the metabolic activity of chondrocytes cultured on the materials using the AlamarBlue cell viability reagent (Invitrogen, Thermo Fisher Scientific, Eugene, OR, USA) according to the manufacturer's guidelines. Briefly, at specific time points (days 1, 4, and 7) the medium was removed from the wells, replaced with a fresh 10% v/v AlamarBlue solution prepared in culture medium, and then incubated at 37 °C in a humidified chamber with 5% CO_2 for 4 h protected from direct light. The fluorescence was measured using an Infinite M200 PRO microplate reader at an excitation/emission wavelength of 560/590 nm. For each experimental group, samples without seeded cells were used as blank controls. Three replicates ($n = 3$) of each material were analyzed, and the fluorescence values of the individual samples were read in triplicate.

Cell Viability and Morphology Observation: The viability of chondrocytes on the materials after 7 days of culture was confirmed by Calcein (ThermoFisher, Waltham, MA, USA) live cell staining (green). For this purpose, samples were washed once with PBS and incubated in a 2×10^{-3} M calcein AM solution prepared in PBS for 1 h at RT and protected from light. The samples were then washed with PBS and immediately imaged with a LEICA DMI3000B fluorescence microscope. The morphology and distribution of cells across the materials' surface was observed by bright-field microscopy, fluorescence microscopy after nuclear staining with 4′,6-diamidino-2-phenylindole (DAPI) dihydrochloride (purity ≥98%, Sigma-Aldrich), and SEM. To perform the DAPI staining, samples were washed twice with PBS, fixed with 4% w/v paraformaldehyde (PFA, Sigma-Aldrich) for 30 min and then permeabilized with 0.1% v/v Triton X-100 (Sigma-Aldrich) for 10 min. The samples were then rinsed twice with PBS and the cells were stained for 5 min with a DAPI solution at 1.5 µg mL^{-1} prepared in PBS. After washing again with PBS, the blue-fluorescent nuclear staining of the cells was observed on a LEICA DMI3000B fluorescence microscope. For SEM imaging, cells were fixed with 4% w/v PFA for 30 min, washed thoroughly with PBS, dehydrated using gradient ethanol solutions, dried at RT, and coated with a thin layer of Au-Pd, in the listed order (see Section 4.3.1).

Alcian Blue Staining and Sulfated Glycosaminoglycan (sGAG) Quantification Assay: The ability of the materials to support chondrocyte differentiation and cartilage extracellular matrix (ECM) production was assessed after 7 days by using the Alcian Blue staining protocol. The cell-seeded hydrogels were washed twice with PBS and fixed with 4% w/v PFA for 30 min. The samples were then washed again with PBS and incubated in a 1% w/v Alcian Blue 8GX (Sigma-Aldrich) solution prepared in 0.1 N hydrochloric acid (Sigma-Aldrich) for 1 h at RT. Afterward, the samples were rinsed with PBS and distilled water twice with each and then imaged with a LEICA DMI3000B microscope equipped with a Nikon DXM1200F digital camera. The sGAG content on the different hydrogel materials was quantified using the Alcian Blue dye precipitation method according to previously reported protocols.[59,60] Briefly, samples stained with Alcian Blue were incubated in 2% w/v sodium dodecyl sulfate (Sigma-Aldrich) overnight in an orbital shaker at 150 rpm. The resultant solutions were read spectrophotometrically with an Infinite M200 PRO microplate reader at 620 nm and the absorbance values were compared to a calibration curve (previously obtained from various dilutions of chondroitin sulfate solutions) to estimate the amount of sGAG in each sample. At least three replicates ($n = 3$) per experimental group were considered and the absorbance of each was measured in triplicate. Samples without seeded cells of each type of material, were subjected to the same protocol and used as blank controls for the absorbance measurements.

2.3.8. Drug Loading and Release

Before the loading/release experiments, the sample disks (Ø6 mm) were dried at 37 °C under vacuum for 48 h, and their weight was measured for further calculations. Drug loading was performed by direct immersion of the materials in drug solutions (5 mg mL^{-1} in PBS) of diclofenac sodium salt (purity ≥98%, Sigma-Aldrich) or ketorolac tris salt (purity ≥98%, ChemCruz, Santa Cruz Biotechnology, Dallas, TX, USA), respecting a ratio

of 0.05 mL mg^{-1} of dry specimen. After 24 h, the samples were sterilized in the loading solutions by autoclaving under the conditions described in Section 4.2 and then stored in these for 1 week at RT (25 °C). For the in vitro drug release assays the loaded disks were immersed in 3 mL of PBS and left in an Incubating Mini Shaker (VWR International, Alfragide, Portugal) at 37 °C and 180 rpm. At selected time points, aliquots of 0.3 mL were collected and replaced with the same volume of fresh PBS. The absorbances of the aliquots were measured at 276 nm (diclofenac) and 324 nm (ketorolac) using a Multiskan GO spectrophotometer (Thermo Fisher Scientific, Kandel, Germany). Calibration curves were obtained for each drug to estimate the amount of drug released from the materials. Once most of the drug was released, each disk was transferred to 3 mL ethanol (37 °C, 260 rpm) to extract the remaining drug. The ethanol solutions were analyzed following a similar procedure as described above (calibration curves were obtained in ethanol) and exchanged daily for new ones until the drug was no longer detected. All conditions were tested twice in quadruplicate ($n = 8$).

2.3.9. Statistical Analysis

IBM SPSS Statistics, version 25 (IBM Corporation, Armonk, NY, USA) was used to perform the statistical analyses. Results are expressed in terms of mean ± SD. To verify normality and homogeneity of variances, data were submitted to Shapiro–Wilk and Levene's tests, respectively. When the assumptions were validated, multiple groups were compared using one-way ANOVA followed by Dunnett's or Tukey's HSD post hoc tests. In cases where the variances were different, Welch's ANOVA and Dunnett's T3 tests were carried out. For normal distributions, independent samples *t*-tests were also conducted to compare means between two groups. Kruskal–Wallis and Dunn–Bonferroni tests were performed when the normality was rejected. The significance level was set at $p < 0.05$ for all tests.

3. Results and Discussion

3.1. Preparation and Morphology of Samples

The treatment of PVA powder and PBO fibers with strong acids resulted in homogeneous solutions, which were used alone or combined to obtain the PVA hydrogels, PBO nanofiber films, and PVA–PBO composites. The dissolution process involved the esterification of the hydroxyl groups of PVA[61] and the gradual protonation of the oxygen and nitrogen atoms on the PBO backbone reducing the intermolecular attractions and chains' stiffness[47,62] (chemical structure of the repeating units of both polymers is given in Figure S1 of Supporting Information).

Preliminary experiments have shown that the duration of the polymers' dissolution process, as well as the concentration of the respective solutions, are critical parameters in the production of the PVA–PBO samples (further details are provided in Section SA of Supporting Information). Upon mixing PVA with PBO, all blends started to gel very quickly, revealing a strong interaction between the two components. The apparent gelation times were not measured, but it was noted that they were shorter the higher the concentration of nanofibers. Typically, one minute after blending the polymeric solutions, which were immediately poured into the glass plates, it was no longer possible to remold any of the prepared compositions without compromising the final form of the materials.

Figure 1 shows digital images of the fabricated samples in the water-swollen equilibrium state. The individual processing of PVA and PBO resulted in the formation of clear and colorless hydrogels and dark goldenrod nanofiber films, respectively. The mixture of both originated composites with colors ranging from yellow to rusty red with an optical clarity that decreases with the increasing concentration of nanofibers. No discernible aggregation or precipitation of the nanofibers in the PVA–PBO samples occurred due to the rapid gelation. However, the size of the hydrated composites was shrunk down (from ≈Ø50 up to ≈Ø40 mm, both ≈2 mm thick) with the incorporation of increasing amounts of nanofibers (from ≈3.2 wt% in 30P1Z up to ≈18.2 wt% in 4.5P1Z), suggesting a crosslinking effect of PBO on PVA.

FEG-SEM imaging was conducted on the materials, which were freeze-dried for observation. The *t*-butyl alcohol method[57] was used to preserve the materials' structure and minimize the appearance of artifacts caused by freezing and drying. SEM micrographs of the cross-sections of PBO films confirmed that Zylon fibers were successfully exfoliated, giving rise to PBO nanofibers with a wide diameter range, up to about 200 nm (**Figure 2**a,b) as observed in other studies.[47,63] The images clearly showed a highly microporous 3D network, with multiple interconnected and randomly distributed fibrils comparable to the structure of cellulose[64] and aramid[11] nanofibers. Cross-sectional and surface images of the PVA hydrogel exhibited a compact structure with a relatively smooth fracture surface (Figure 2c) but with some protuberances on the surface of the material (Figure 2d). Concerning the composites, since the SEM micrographs were similar for the different formulations, only those of 6P1Z are provided (Figure 2e,f). The inner surface of the composite evidenced good embedding and homogeneous distribution of the nanofibers into the hydrogel matrix, with some fibrils that were broken as a result of fracturing (Figure 2e). In contrast, the outer surface of the composite was shown to be quite smooth and uniform (Figure 2f). Both images of 6P1Z further indicate excellent interfacial adhesion between PBO and PVA and a continuous nature of the polymeric matrix.

3.2. Chemical and Thermal Characterization

Infrared spectroscopy was used to confirm the regeneration of PBO nanofibers after the downsizing treatment and to study the chemical characteristics of the materials produced. **Figure 3**a shows the attenuated total reflectance Fourier transform infrared (ATR-FTIR) spectra of the PBO fibers before and after the exfoliation process. The spectrum of Zylon commercial fibers exhibited typical absorption peaks[47,65–69] ascribed to the following vibrations: 1617 cm^{-1} (C=C stretching of aromatic rings and C=N stretching in cyclic compounds); 1552 and 1490 cm^{-1} (stretching vibration of unsaturated C–C on the benzene ring); 1409, 1360, and 1307 cm^{-1} (C–N stretching); 1270 cm^{-1} (C–C stretching of the carbons linking the oxazole and the phenyl ring and O–C=N stretching); 1110 and 1007 cm^{-1} (in-plane C–H bending

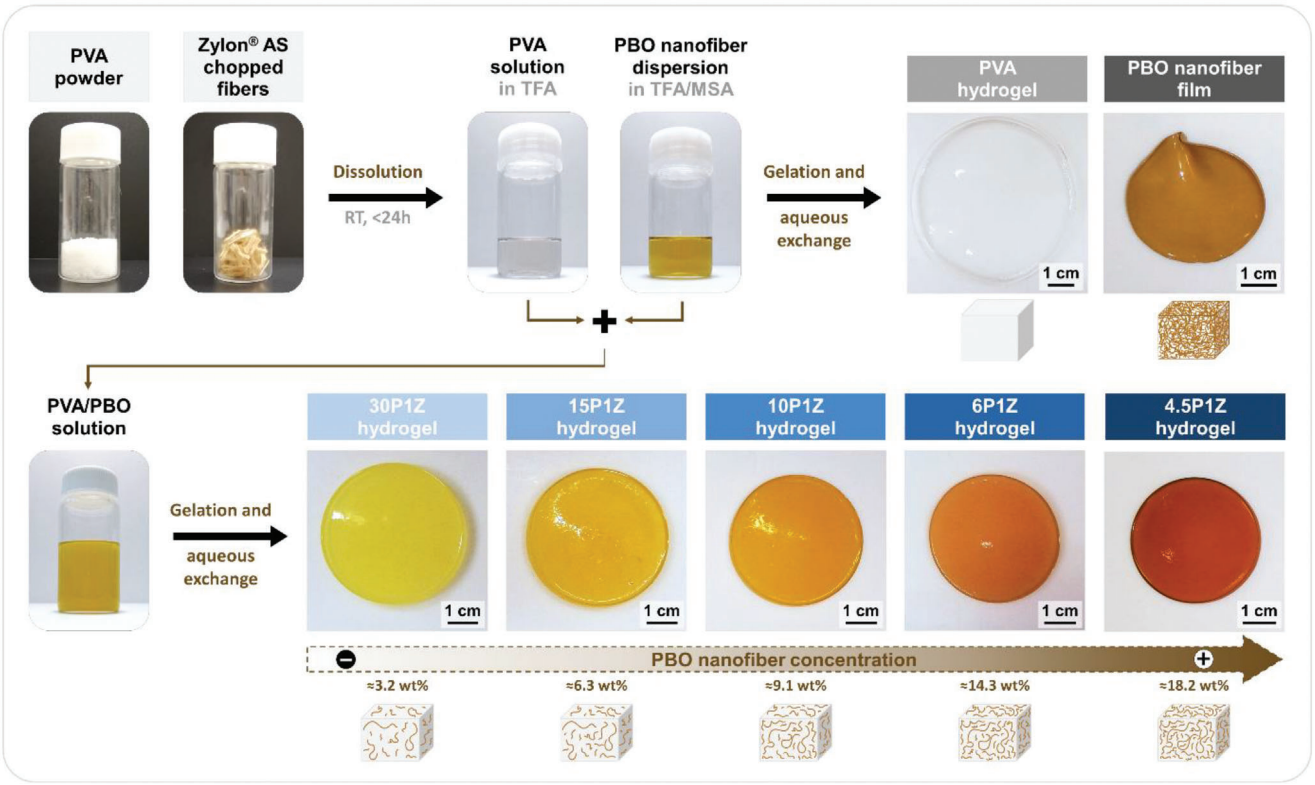

Figure 1. Schematic representation of the samples' preparation with photographs of typical solutions and materials produced.

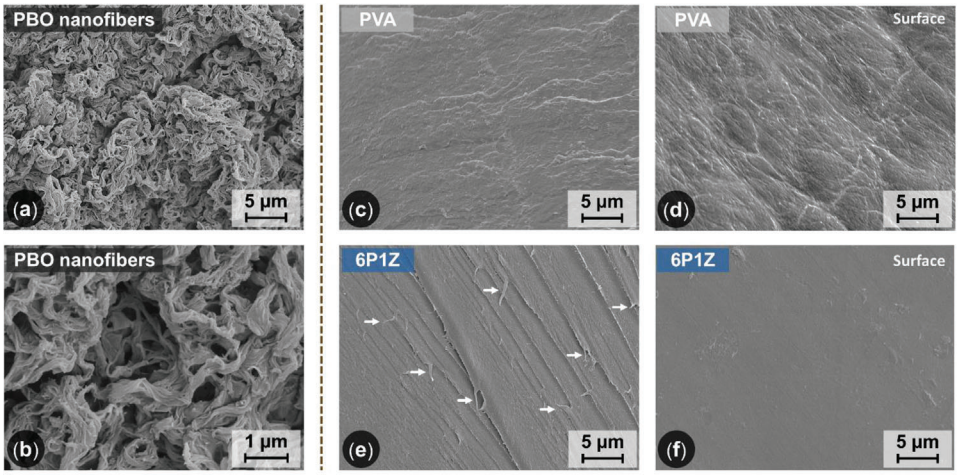

Figure 2. Cross-sectional SEM images of PBO nanofiber films a,b), PVA c), and 6P1Z e). SEM images of the surface of PVA d) and 6P1Z f). The white arrows indicate the location of some of the nanofibers incorporated within the 6P1Z composite.

of aromatic rings); 1046 cm^{-1} (C–O–C stretching in oxazole ring); 921 cm^{-1} (symmetric C–O–C stretching of a cyclic ether); and 840, 820, and 697 cm^{-1} (out of plane C–H bending of aromatic rings). As for the PBO nanofibers, the spectrum was very similar to that of commercial fibers, except for some minor peak shifts and intensity changes, indicating that the molecular integrity of PBO was well preserved. The variations might be attributed to differences in fiber alignment[47,63] between the highly oriented PBO chains[70] in the Zylon yarns and the randomly distributed nanofiber networks. Also, a partial hydrolysis of the oxazole ring might have occurred, with the formation of carboxyl, amino, and phenolic hydroxyl groups (increase of the peak between 1410 and 1310 cm^{-1}).[63,71]

ATR-FTIR spectrum of the composite 6P1Z (taken as an example) is presented in Figure 3b along with that of PBO nanofibers and PVA. It is worth noting that none of the spectra of the

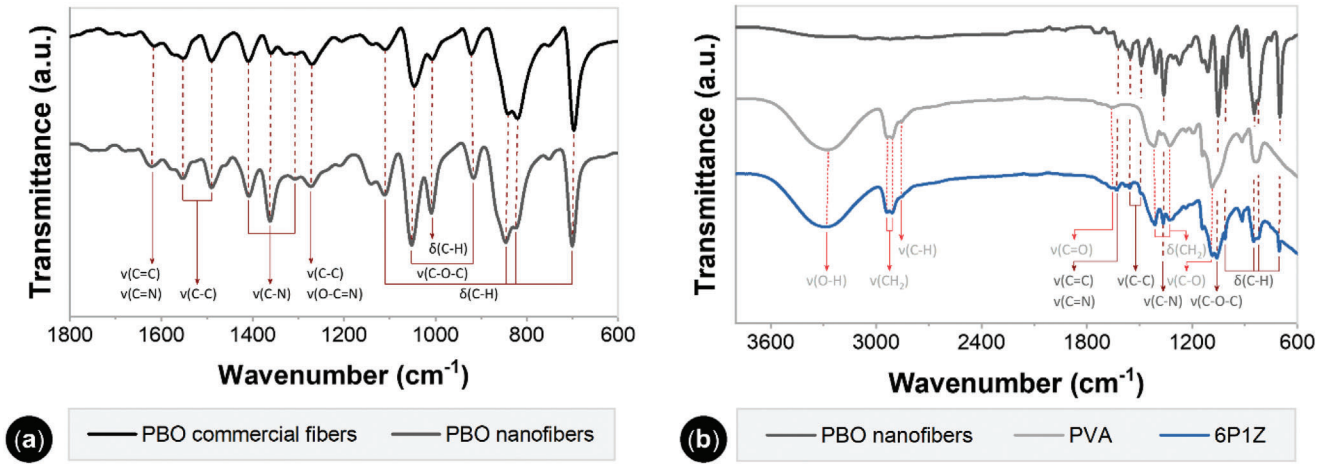

Figure 3. ATR-FTIR spectra of PBO commercial fibers and nanofibers a). ATR-FTIR spectra of PBO nanofibers, PVA, and 6P1Z b). Abbreviations: v, stretching; δ, bending.

materials showed any trace of the solvents used, demonstrating that the methodology used for their removal was effective. In fact, the main vibrations of TFA,[72] that typically occur at 1785 cm^{-1} (C=O stretching) and 1225 and 1165 cm^{-1} (asymmetric and symmetric stretching of CF_3, respectively) and those of MSA,[73] that appear at 1320 and 1122 cm^{-1} (asymmetric and symmetric SO_3 stretching, respectively), 886 cm^{-1} (S–OH stretching), and 763 cm^{-1} (C–S symmetric stretching) were not observed. In the case of PVA, typical vibrational peaks[72,74] occurred at 3272 cm^{-1} (O–H stretching), 2937 and 2909 cm^{-1} (asymmetric and symmetric CH_2 stretching modes, respectively), 2856 cm^{-1} (symmetric C–H stretching), 1659 cm^{-1} (C=O stretching of residual vinyl acetate groups), 1417 and 1327 cm^{-1} (CH_2 bending), and 1086 cm^{-1} (C–O stretching). For 6P1Z, the bands were attributed to the characteristic absorption peaks of its two constituents, with a strong contribution from PVA, which is in greater quantity, but well-defined peaks ascribed to the PBO nanofibers, as well. Apart from the additive effect of the two polymers, no other significant changes were observed in the spectrum of 6P1Z that provide evidence on the type of interactions established between PVA and PBO. However, as observed in the spectrum of acid-treated PBO and similarly reported in other research works, 2-phenylbenzoxazoles can be hydrolyzed[67] in acidic medium[63,75] leading to the formation of carboxyl, amino, and phenolic hydroxyl groups. Thus, the newly formed functional groups can establish intermolecular hydrogen bonds between the PBO nanofibers, as well as between them and PVA,[63] which are not detectable by FTIR spectroscopy. Therefore, besides the physical interactions between PVA chains (H bonds) or PBO fibrils (van der Waals[47] and H bonds), the strong intermolecular hydrogen bonds between PVA and PBO also play a role, becoming the primary driving force for the formation of PVA–PBO composites.

TGA and DSC techniques were used as complementary methods to probe thermal information on the materials. The assays were performed on PBO nanofiber films, PVA, and 6P1Z (taken as representative), and the results obtained are displayed in **Figure 4**. The TGA thermogram and derivative thermogravimetric (DTG) curve for the PBO nanofibers revealed that no obvious weight loss took place below 600 °C (Figure 4a,b) and DSC analysis proved the absence of any phase change up to 240 °C (Figure 4c–e). These findings confirm the excellent thermal stability of PBO nanofibers, enabled by the presence of the phenylene and oxazole rings in the backbone, and are consistent with previous reports.[47,65,68] As for PVA, the TGA and DTG graphs showed four main regions that relate to three distinct degradation processes (stages), as in other observations,[76,77] while the composite 6P1Z presented only three zones that correspond to the same degradation events (Figure 4a,b). In both samples, the first recorded weight losses had maximum rates at 117 °C for PVA and 171 °C for 6P1Z and were attributed to evaporation of water and/or residual solvents (moisture).[41,63,76–78] At this stage, the total moisture content was similar for PVA (7 wt%) and the composite (8 wt%). However, its release kinetics was slower for 6P1Z compared to PVA (80–150 °C), as it occurred over a wider temperature range (85–215 °C), which implies that PBO must have helped to retain and hinder the removal of water molecules. The 10% loss was observed at 272 °C for PVA and 322 °C for 6P1Z. Two well-separated inflections characterized the second degradation stage of PVA with maximum peaks at 278 and 370 °C and with weight losses around 17 and 45 wt%, respectively. In turn, for 6P1Z the second degradation region was marked by the existence of a single sharp peak at 376 °C associated with a weight loss of about 46 wt%. This second event was responsible for the greatest mass loss in both materials and was ascribed to the degradation of the hydroxyl side groups of PVA[41,76,78] with the formation of polyenes.[79] In the last stage of thermal decomposition, the rate was maximum at 427 °C for PVA and 430 °C for 6P1Z and involved a weight loss close to 28 wt%. in each material owing to the breakdown of the PVA backbone (CH_2–CH_2)[41,76,79] that resulted in the formation of carbon and hydrocarbons.[41] At 600 °C, the amount of solid residue of 6P1Z was substantially higher (17 wt%) than that of PVA (3 wt%) due mostly to the presence of the thermally resistive PBO.

The disappearance of the first peak of the second stage of PVA degradation in the composite, the shift of all remaining peaks to higher temperatures, and the larger amount of final residue clearly support that the addition of PBO effectively improved the thermal stability of PVA. This improvement could be the result

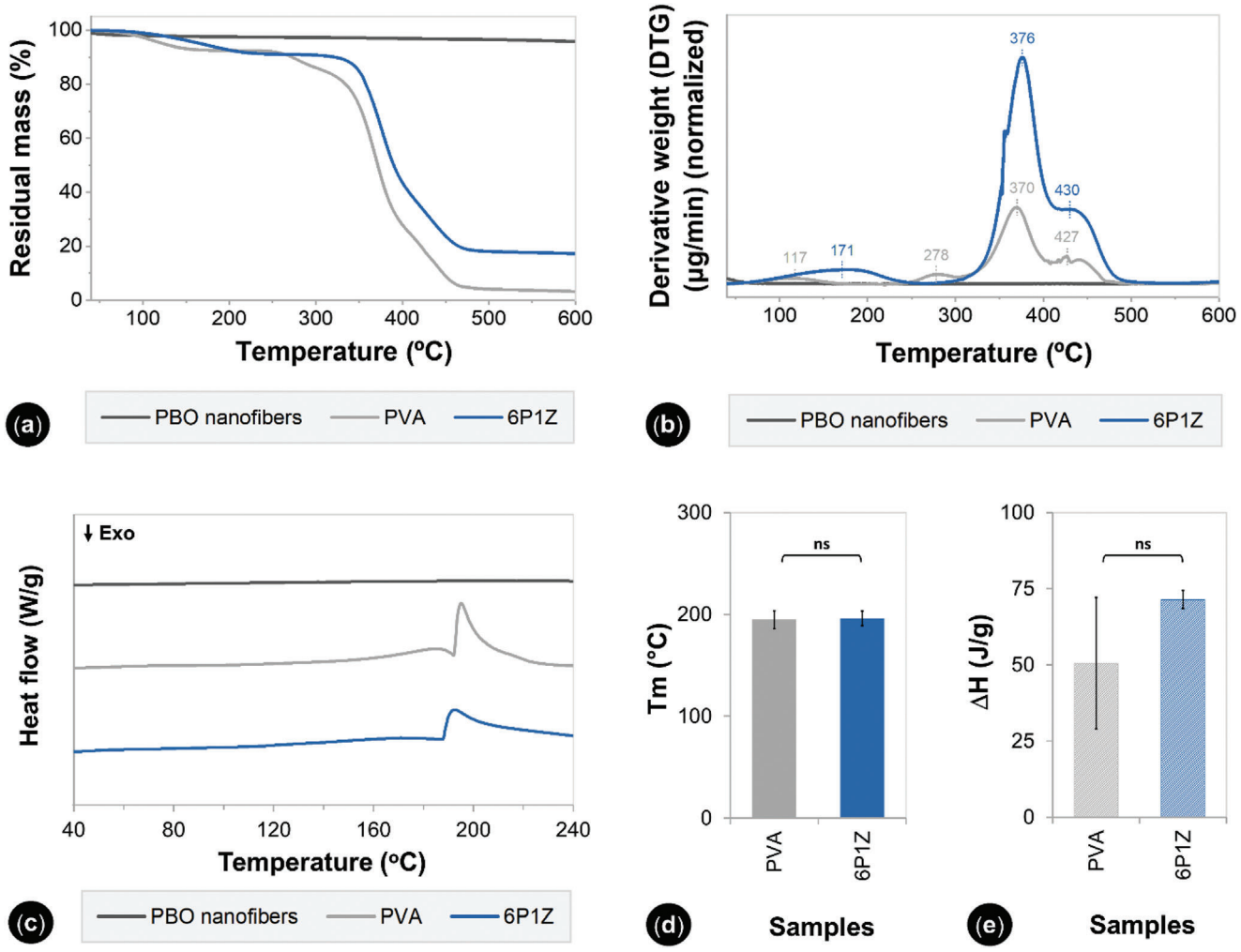

Figure 4. TGA thermograms of PBO nanofiber films, PVA, and 6P1Z a) and respective derivative curves b). DSC thermograms of PBO nanofiber films, PVA, and 6P1Z c) and corresponding values of the melting temperature peaks d) and fusion enthalpies e). The error bars correspond to ± SD. For the melting temperature and fusion enthalpy data, pairwise comparisons between groups were performed using the independent samples *t*-test. "Ns" indicates a nonsignificant difference ($p \geq 0.05$).

of the strong intermolecular hydrogen bonds between PVA and PBO nanofibers, which slow down the degradation of PVA.[80]

Contrarily to what would be expected considering the likely increase in secondary hydrogen bonds, the DSC curves for PVA and 6P1Z, and the corresponding values of melting temperature (T_m) and heat of fusion (ΔH) revealed that there were no significant changes between the two materials (Figure 4c–e). No glass transition temperature was detected in the temperature interval analyzed and the only endothermic melting peak occurred in the 188–202 °C range in both samples, in agreement with typical values reported for PVA,[19,72,78] indicating that the crystallinity was similar between the two materials. Still, it is important to mention that, unlike the composite whose DSC thermograms showed a high reproducibility, some variability was obtained in the shape and amplitude of the melting peaks of the DSC curves acquired for the six PVA replicates tested, mostly affecting the heat of fusion values. This was probably due to the proximity to the onset degradation temperature of the O–H side groups of PVA in the unmodified sample.

3.3. Physical and Mechanical Characterization

The equilibrium water content of the materials was investigated, and the results are summarized in **Figure 5**. There was an initial trend of higher water content values for the composite with the lowest amount of PBO (30P1Z), followed by a gradual decrease as the PBO nanofiber content increased in the hydrogel composites. This effect was however more pronounced with respect to swelling (see Figure S2 in the Supporting Information), which confirms to some extent, the previously observed trend of decreasing sample size as a function of increasing nanofiber concentration. In comparison to PVA, a significant reduction in the water content was evident in the two materials containing the highest concentration of reinforcing agent (6P1Z and 4.5P1Z), most probably due to the inability of PBO to form hydrogen bonds with water[67] and the likely increase in the number of crosslinks that should have restricted the chains' mobility[81] in the polymer network. As a matter of fact, it is well known that the water content and swelling of hydrogels depend mainly on the

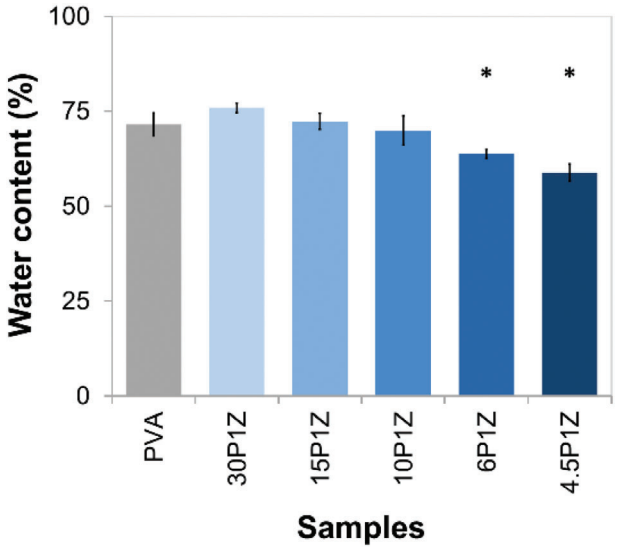

Figure 5. Water content of the materials in the equilibrium state. The error bars correspond to ± SD. Statistical significance was calculated by ANOVA and Dunnett tests. The asterisk (*) indicates the statistical difference for the comparison between samples without nanofibers (PVA—control group) and with different PVA:PBO nanofiber mass ratios ($p < 0.05$).

hydrophilic capacity of functional groups and the crosslinking density.[25,37] Since the materials produced are intended to replace cartilage, the water content should ideally be within the range of values found in cartilaginous tissues (60–80%).[19,82,83] Compliance with this requirement is essential to ensure cell viability[84,85] and viscoelastic propensity.[86] In this regard, we chose not to add more PBO (max. 18.2 wt%) to avoid an unfavorable decline in the water absorption properties of the composites.

A later study was conducted on the swelling ability of 6P1Z using different buffer solutions at pH 4, 7, 9, and 12, which revealed that the PVA–PBO composite is sensitive to this parameter. In fact, with increasing pH, the swelling (and the typical coloration of the material—see Section 2.1) varied as follows: 183% (bright light orange) > 170% (burnt orange) < 195% (rusty red) < 210% (dark red). It is therefore important to consider this pH dependence in future studies, as both swelling, and swelling-dependent properties may differ from those obtained in this work. This pH responsiveness characteristic can also be of great utility in many other hydrogel applications such as for epidermal wound monitoring[87] and in actuators[88] and sensors,[89] just to name a few.

To evaluate the reinforcing effect of the PBO nanofibers, the mechanical performance of the PVA–PBO composites was investigated and compared to that of PVA. The typical tensile and compressive stress–strain curves acquired are displayed in **Figure 6**a,c, from which the properties have been summarized in **Table 1**. The elastic moduli determined for the lowest strain values are also shown in Figure 6b,d. Regarding tensile behavior, the increased content of embedded nanofibers led to obvious improvements in stiffness, strength, and toughness. The elastic moduli of all materials were higher in the initial phase and then trended toward an approximately constant value throughout the elongation path. This modulus reduction during stretching should be caused by the outflow of water from the hydrogel network and the alignment of the PVA and PBO chains in the stretching direction. Elongation at break was also significantly enhanced in samples 15P1Z, 10P1Z and 6P1Z, which indicates that despite the relatively high concentration of stiff nanofibers (6.3–14.3 wt%), the extensibility limit was not adversely affected. The 6P1Z composite showed a superior toughness than that observed in the sample with the highest nanofiber content as a result of greater extensibility. In addition, 6P1Z achieved an elastic modulus, elongation at break, tensile strength, and toughness corresponding to 7.0×, 1.4×, 2.5×, and 4.0× more than in PVA.

A similar behavioral pattern was observed in the composites subjected to compression. The materials became stiffer (modulus increased) and less compressible (strain decreased) by adding increasing amounts of PBO. The compression moduli were roughly constant, with a slight tendency to increase over the strain range up to 20%, with the exception of 4.5P1Z where such increase was more pronounced. The incorporation of nanofibers also caused an increase in the energy dissipation capacity of the materials, even though the determined percentages of dissipated energy decreased at the expense of higher stiffness and lower compressibility. In fact, the composites with more PBO absorbed more energy for a given applied strain and are also expected to dissipate more during unloading, which supports the hypothesis that PVA–PBO hydrogels might have a strain-dependent energy dissipation behavior.[20] Additionally, the composites exhibited rapid self-recovery properties at RT, reaching 98–100% of their original height after 30 min of resting in water, indicating that the deformation induced in the material structure by the compressive effort had a reversible character.

Overall, the mechanical results agree with those we obtained previously since higher strength and stiffness are often associated with increased thermal stability[77] and a lower hydration capacity.[27,37] Among the PBO contents used, 6P1Z was shown to have the mechanical properties most similar to those of natural cartilage. The tensile modulus (at 8% strain)[90,91] and ultimate tensile strength[92] of articular cartilage are typically within the ranges of 3–13 and 6–14 MPa respectively, while its compressive modulus (in unconfined mode at 10–20% strain)[22,51,93,94] is between about 1.5 and 3.0 MPa. The extraordinary mechanical properties of the PVA–PBO not only stem from the high intrinsic strength of PBO[47] but shall also be attributed to the slightly increased solid content, the good dispersion and high aspect ratio of the nanofibers in the hydrogel matrix, the optimal interfacial adhesion between the two components, and the increased number of intermolecular hydrogen bonds between PVA and PBO. The strength mechanism of our composites was also more effective than others observed in the reinforcement of PVA with cellulose[20,95] or aramid[11] nanofibers.

An evaluation of the mechanical behavior under dynamic conditions was also performed on sample 6P1Z, which was subjected to 100 consecutive compression cycles up to a maximum strain of 30%. The results obtained are shown in **Figure 7**a,b. A decrease in the maximum stress was observed with increasing the number of cycles, tending to an asymptotic value around 0.55 MPa after 80 cycles. At the end of 100 compression cycles, no cracks or permanent damage was detected on the surface of the material, only a reduction of about 11.5% in the samples' height was recorded, which was fully recovered in less than 24 h after resting in water.

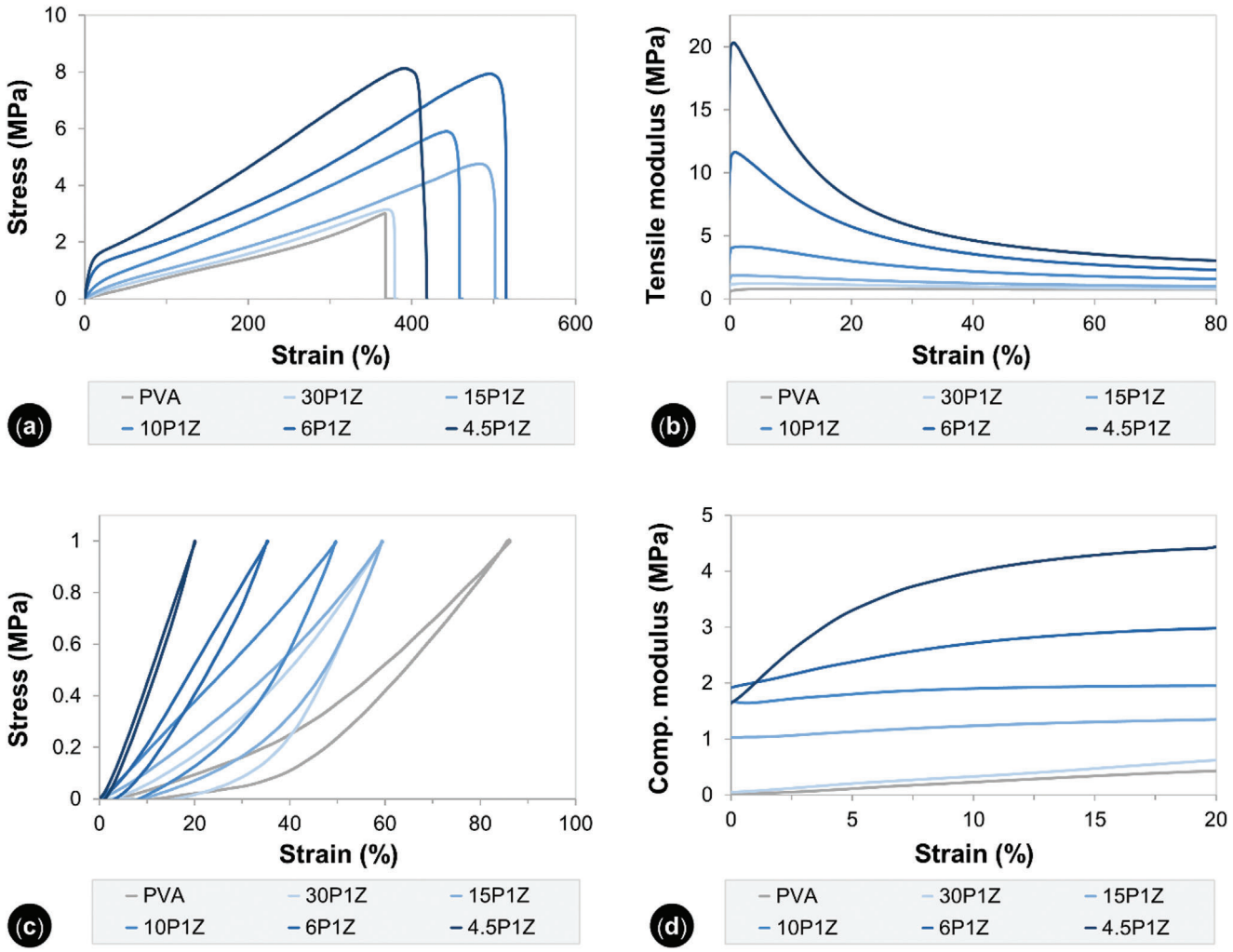

Figure 6. Mechanical characterization of PVA and nanofiber-reinforced hydrogels with different PVA:PBO nanofiber mass ratios. Typical tensile stress–strain curves a) and corresponding values of tensile moduli up to 80% of strain b). Typical compressive stress–strain curves c) and corresponding values of compression moduli up to 20% of strain d).

Table 1. Tensile and compression properties of PVA and nanofiber-reinforced hydrogels with different PVA:PBO nanofiber mass ratios. Data are presented as means ± SD. Statistical significance was calculated by ANOVA and Dunnett tests. The asterisk (*) indicates the statistical difference for the comparison between samples without nanofibers (PVA—control group) and with different PVA:PBO nanofiber mass ratios ($p < 0.05$).

Sample	Tensile properties			Compression properties	
	Elongation at break [%]	Tensile strength [MPa]	Toughness [MJ m^{-3}]	Strain [%]	Dissipated energy [%]
PVA	385 ± 53	3 ± 1	6 ± 2	85 ± 5	19 ± 3
30P1Z	390 ± 52	3 ± 1	6 ± 2	62 ± 4 (*)	38 ± 2 (*)
15P1Z	504 ± 73 (*)	4 ± 1	11 ± 5	57 ± 2 (*)	38 ± 6 (*)
10P1Z	479 ± 51 (*)	6 ± 1 (*)	15 ± 4 (*)	48 ± 2 (*)	36 ± 3 (*)
6P1Z	518 ± 33 (*)	8 ± 1 (*)	22 ± 4 (*)	33 ± 3 (*)	20 ± 1
4.5P1Z	406 ± 54	8 ± 2 (*)	19 ± 6 (*)	23 ± 3 (*)	13 ± 2 (*)

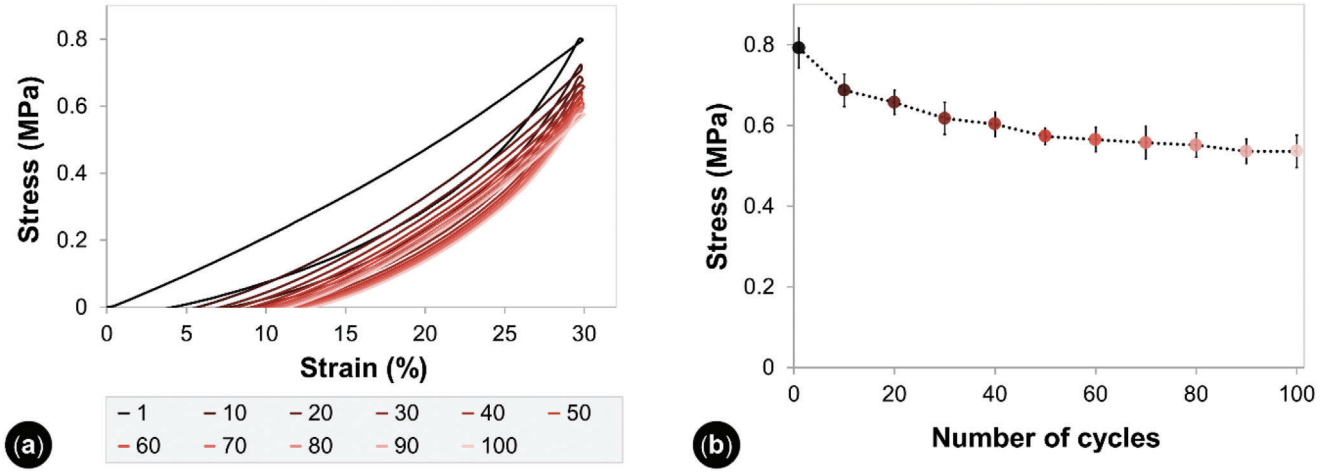

Figure 7. Compressive behavior of sample 6P1Z under dynamic conditions. Typical compressive stress–strain curves at selected cycles a) and corresponding stress values at 30% strain as a function of the number of cycles b). The error bars correspond to ± SD.

3.4. Effects of Sterilization

Sample 6P1Z was selected to study the effect of sterilization on the properties of PVA–PBO composites, as it combined a water content closer to that of cartilaginous tissue with exceptional mechanical performance. Two conventional methods, widely used in the terminal sterilization of medical devices, were employed: 1) steam heat (autoclaving) and 2) gamma radiation. For the former, the hydrogels were autoclaved in the hydrated condition in a specific amount of water, while for the latter, the composites were irradiated in the dry state. The use of dry samples in the irradiation procedure was due to the fact that hydrogels are more prone to degradation when exposed to gamma radiation in the presence of water, owing mainly to free radical formation.[96] The effect of the sterilization procedures on the materials (herein designated as 6P1Z_AUT and 6P1Z_GR) was determined by comparison of the performance of the sterilized and nonsterilized composite (6P1Z). The results obtained regarding the thermal behavior, water content, swelling, and mechanical properties are shown in Figures S3 and S4 in the Supporting Information.

On the basis of macroscopic observation, no changes were seen in the color, shape, or size of the materials after sterilization. More importantly, unlike pure PVA hydrogels[25] and many PVA-based composites that redissolve above 60–70 °C, no evidence of redissolution occurred in the samples autoclaved at 121 °C. This ability to resist autoclaving should be associated with the establishment of the noncovalent secondary interactions (hydrogen bonds) between the PVA and PBO chains. A similar phenomenon is known in nylon (polyamide),[97,98] where the presence of secondary hydrogen bonds between the amide groups of the molecular chains is responsible for the higher chemical, mechanical and thermal resistance of the material. Regarding FTIR, the spectra revealed minor variations in the intensity of the peaks corresponding to the PVA segments (see Section 2.2) in 6P1Z_AUT (Figure S3a, Supporting Information). Additionally, 6P1Z_GR exhibited a slight increase in the intensity of the vibrational peaks 2939 and 2911 cm^{-1} assigned to the asymmetric and symmetric CH_2 stretching modes of PVA. No changes were observed in the DSC thermograms of the sterilized samples compared to the nonsterilized one (Figure S3b–d, Supporting Information). As for water content and swelling, 6P1Z_GR presented lower values than 6P1Z or 6P1Z_AUT (Figure S4a,b, Supporting Information). The mechanical behavior in both tensile and compression regimes was consistent in the sterilized and nonsterilized composites (Figure S4c–f, Supporting Information), with none of the corresponding properties being statistically impacted (Table S1, Supporting Information). Overall, both sterilization methods proved to be suitable for the PVA–PBO composites and did not significantly impair the analyzed properties. However, considering the mildly better performance of 6P1Z_AUT in which none of the thermal, physical, and mechanical properties were affected, the easier access to an autoclave, and the possibility of performing terminal sterilization of the material in the hydrated form, the steam heat sterilized sample was chosen to proceed with the study.

3.4.1. Tribological Behavior

Any cartilage replacement material should have a low coefficient of friction (CoF) and high resistance to wear to prevent the opposing cartilage from wearing away and ensure adequate performance and durability.[10,99] The CoF and wear resistance of PVA and 6P1Z_AUT samples were determined by reciprocating linear motion of a stainless-steel ball on top of the materials immersed in a PBS solution. Increasing loads ranging from 5 to 30 N were applied, corresponding to contact pressures in the range of 1.2–2.2 MPa as estimated by Hertzian theory.[100] The kinematic and loading conditions were chosen based on the typical average values of sliding velocity[101] and contact stress[102] found in the human hip joint cartilage during normal walking. The results obtained as a function of the applied load are shown in **Figure 8**.

It can be seen that both the CoF and wear loss of the two types of samples increased with the normal load. This is because, like cartilage, PVA hydrogels are highly resilient and viscoelastic biphasic materials (consisting of a solid and a fluid phase) that can easily undergo deformation.[27,103,104] As the applied loads increased, more water was squeezed out of the hydrogel net-

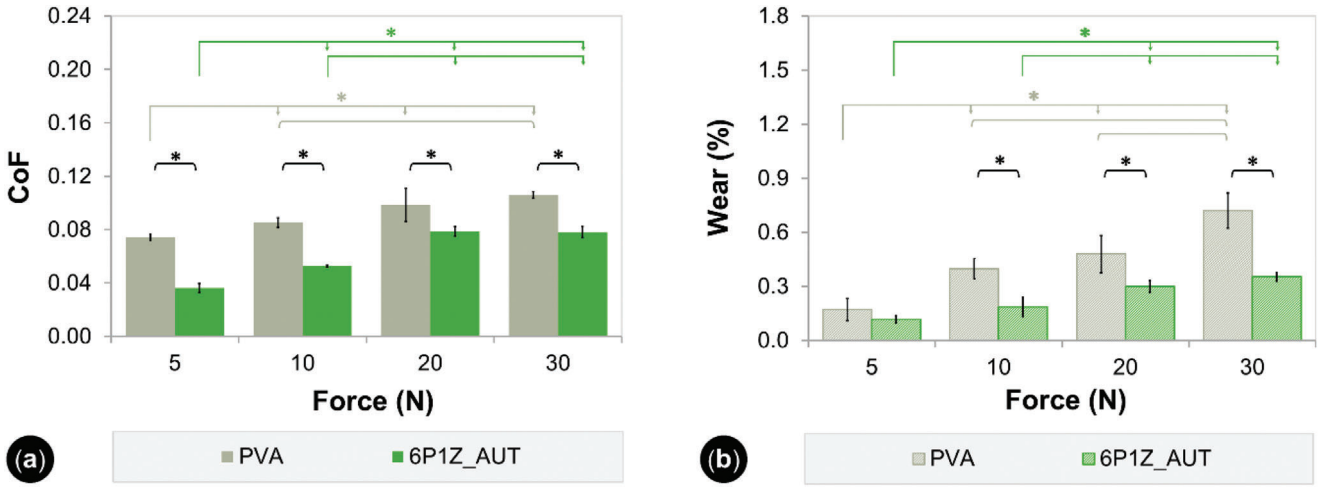

Figure 8. Dynamic friction coefficients a) and wear mass percentages b) of PVA and 6P1Z_AUT samples obtained in the ball-on-plate friction tests under lubricated conditions. The error bars correspond to ± SD. Friction coefficient data were tested by Welch's ANOVA/Dunnett's T3 (PVA under 5, 10, 20 or 30 N), ANOVA/Tukey's HSD (6P1Z_AUT under 5, 10, 20 or 30 N), and independent samples *t*-test (PVA vs 6P1Z_AUT under each of the applied forces). Data from the wear measurements were analyzed by ANOVA/Tukey's HSD (each type of sample under 5, 10, 20, or 30 N) and independent samples *t*-test (PVA vs 6P1Z_AUT under each of the applied forces). Statistical differences ($p < 0.05$) between groups are indicated with an asterisk (*).

works, and greater deformation occurred, leading to an enlargement of the contact area between the sliding pairs and consequently an increase in CoF and wear. Under the same normal load, the composite showed significantly lower CoFs and higher wear resistance than PVA. This improvement in the tribological behavior is attributed to the incorporation of PBO nanofibers that endowed the composite with a more resistant structure and enhanced load-bearing capacity. The higher crosslinking density in 6P1Z_AUT should have limited the conformational adjustments of the polymer chain segments upon deformation, reducing the contact area between the sliding pairs and the shear–tear strength in the contact point. When subjected to the highest load, the CoF of the composite was less than 0.08, and the wear loss did not exceed 0.35%, while for the PVA control sample, the CoF reached 0.1 with a maximum wear percentage of 0.72%. These CoFs are extremely low and are in line with those found for articular cartilage (0.002–0.600).[19,99,104–106] This wide range of reported friction coefficient values is due to the fact that the study conditions are not standardized, and the CoFs strongly depend on the counterbody material, system geometry/configuration, and testing parameters/conditions.[19,104] It should also be noted that the friction tests were performed under harsher conditions than physiological ones, using a steel ball (which is much harder than natural cartilage) and in the absence of synovial fluid components (such as hyaluronan and lubricin) that contribute to the boundary lubrication. It is, therefore, reasonable to expect that the tribological performance of the composite material will be even better when the cartilage-hydrogel pair slides with the natural lubricant.[104]

3.4.2. Biocompatibility

It is a prime requirement that any implantable biomaterial be noncytotoxic so as not to harm surrounding tissues, induce inflammation, or cause a foreign body response. The biocompatibility of 6P1Z_AUT was evaluated using human chondrocytes. Cell viability was assessed after exposure to the leachable extracts of the composite for 48 h using the MTT assay and by direct contact of the material with a confluent monolayer of cells for the same period of time. The percentage of viable chondrocytes was about 100% (**Figure 9**a), and no signs of cytotoxicity or cell death were observed when compared to the control groups (Figure 9b–d).

Numerous authors have already demonstrated that PVA is highly biocompatible,[27,107,108] but little information seems to exist on PBO. Hu et al.[48] observed a good cytocompatibility in NIH/3T3 mouse fibroblasts cultured with extracts of a resin-based endodontic post material reinforced with PBO fibers. Besides this, no other studies have been found in the literature attesting to the biocompatibility of PBO. Here, the absence of an adverse cellular response provided evidence of the biological safety of the PVA–PBO composite as a promising cartilage replacement material.

Cell adhesion and proliferation were assessed by the Alamar-Blue assay method, while chondrocyte differentiation was evaluated by quantifying the amount of sulfated glycosaminoglycans, which are a key component of native cartilage. Cell density and morphology were also investigated using bright-field and florescence microscopy, and SEM. These studies were performed on the 6P1Z_AUT composite material and the results compared to those of a pure PVA sample. As shown in **Figure 10**a, 6P1Z_AUT significantly promoted greater adhesion and proliferation of chondrocytes (on days 1, 4, and 7 of culture) compared to PVA. Cells cultured on the composite achieved a 2.1-fold increase on day 7 relative to day 1, while those cultured on PVA only reached a 1.5-fold increase. These results were supported by the images of phase contrast bright-field microscopy (Figure 10c,g), fluorescent calcein (Figure 10d,h) and DAPI nuclear staining (Figure 10e,i) obtained after 7 days of culture, which suggest a higher number of viable cells present in the PVA–PBO composite. The morphology of chondrocytes cultured on 6P1Z_AUT for

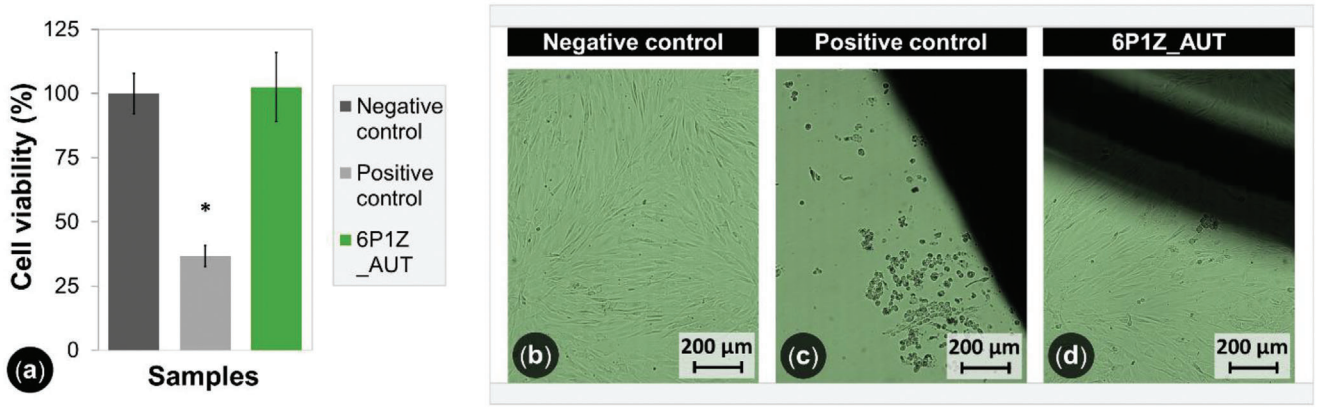

Figure 9. Viability of chondrocytes after 48 h of culture in conditioned medium (MTT assay) a). The error bars correspond to ± SD. Representative images of chondrocytes after 48 h of direct exposure to the materials (direct contact test) b–d). Statistical significance was calculated by Kruskal–Wallis and Dunn–Bonferroni tests. Significant differences ($p < 0.05$) between groups are indicated with an asterisk (*).

7 days was also observed by SEM microscopy (see Figure S5 in the Supporting Information).

Glycosaminoglycans are key components of the cartilage ECM that play a crucial role in the maintenance of tissue homeostasis not only as providers of mechanical resistance to compressive loads, but also due to their participation in different signaling pathways that regulate cellular processes such as cell adhesion, growth and differentiation.[109,110] Thus, due to their biological relevance, the production of glycosaminoglycans has been used as one of the main outcomes to evaluate the ability of materials to support chondrocyte differentiation and generate cartilage-like tissues. As can be seen by Alcian Blue staining in Figure 10f,j, both materials supported the secretion of typical sGAG-rich cartilage ECM. However, the amount of sGAG present after 7 days of culture on the 6P1Z_AUT composite was significantly higher than that obtained in the PVA sample (17 ± 3 µg/scaffold vs 7 ± 1 µg/scaffold) suggesting a better performance of the composites in promoting chondrocyte differentiation and cartilage ECM production (Figure 10b).

3.4.3. PVA–PBO Composites as Drug-delivery Platforms

The use of biomaterials as reservoirs of bioactive molecules can enrich their functionality and broaden their potential applicability. To evaluate the possibility of using PVA–PBO composites as drug delivery platforms, 6P1Z_AUT samples were loaded with the anti-inflammatories diclofenac (DFN) and ketorolac (KTL), medicines that are commonly prescribed for the relief of inflammatory symptoms after an orthopedic surgery, whose local-level vehiculation may bring benefits in terms of efficiency and reduction of side effects.[27,50,55]

After autoclaving the composites in the different loading solutions, the materials were left to load for 1 week. The stability of both drugs in solution after steam heat sterilization has been confirmed in a previous study.[96] The cumulative release profiles of both drugs, represented by the total amount of drug released per mg of dry sample and in percentage terms, are shown in **Figure 11**a,b, respectively.

During the 24 h of the release experiment, the amount of DFN eluted (40 µg mg^{-1}) was about twice that of KTL (21 µg mg^{-1}) (Figure 11a). The same trend was observed in other hydrogels loaded with these drugs.[27,53,111] While KTL release was almost completed in less than 8 h, DFN release was more sustained and occurred for at least 24 h (Figure 11b). A burst effect[112] associated with the diffusion of the drug molecules that were free and loosely bound to the material was observed in both cases. After 24 h about 85% of DFN was released while for KTL a value of 88% was reached in approximately 8 h.

Although the release of DFN was more controlled and prolonged compared to KTL, both drugs were released within a short period (≤24 h). After the repair of a chondral defect, a longer, sustained release of an anti-inflammatory (e.g., 3–5 days) would be more advantageous. However, this was only a screening experiment to evaluate the potential of the material to act as a drug delivery platform. The in vivo conditions shall be quite different in terms of surrounding fluid composition, hydrodynamic conditions, load bearing, etc., and may vary between the different joints. Thus, these results should only be considered in a qualitative manner.

To study the effect of the pH of the loading solution on the release behavior of DFN, experiments were also performed using a DFN loading solution at pH 9, which should not pose any problems in physiological terms and should have a minimal effect on the stability of the drug.[113,114] However, the improvement in the amount and kinetics of DFN release turned out to be very small (data not shown). Other approaches regarding the incorporation of drugs into PVA–PBO hydrogel composites should be considered in future studies. Some examples include modifying the loading conditions,[111] using different loading techniques,[115] or alternative drugs that promote specific interactions between the drug and the material that help control and extend drug release.

3.5. Effect of Reinforcement on Water-Free Materials

To infer about the potentiality of using the new PVA–PBO materials in the dry form in other different applications, the effect

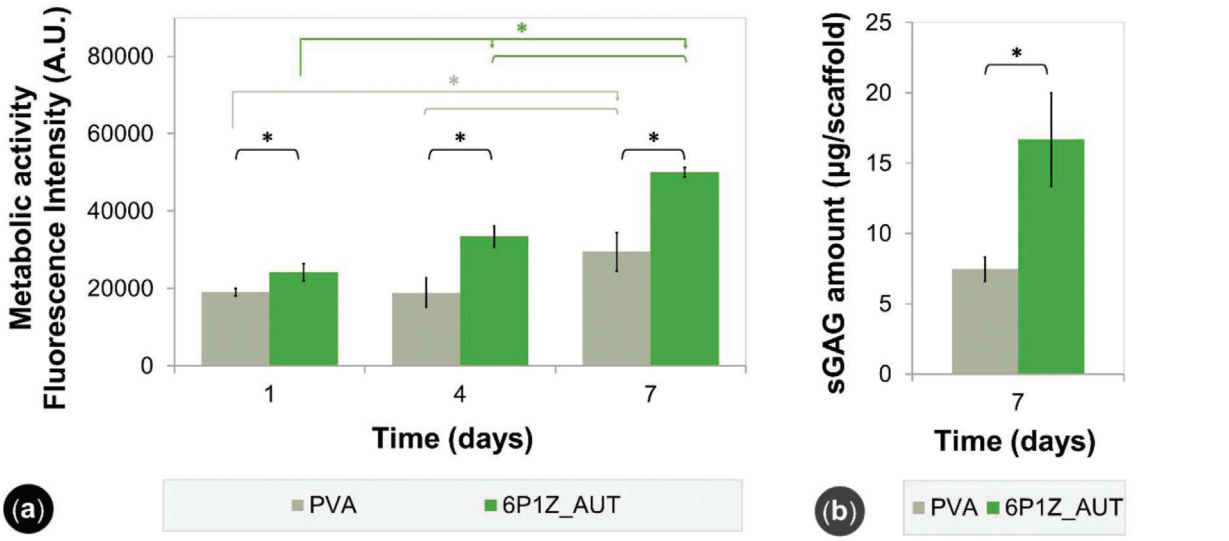

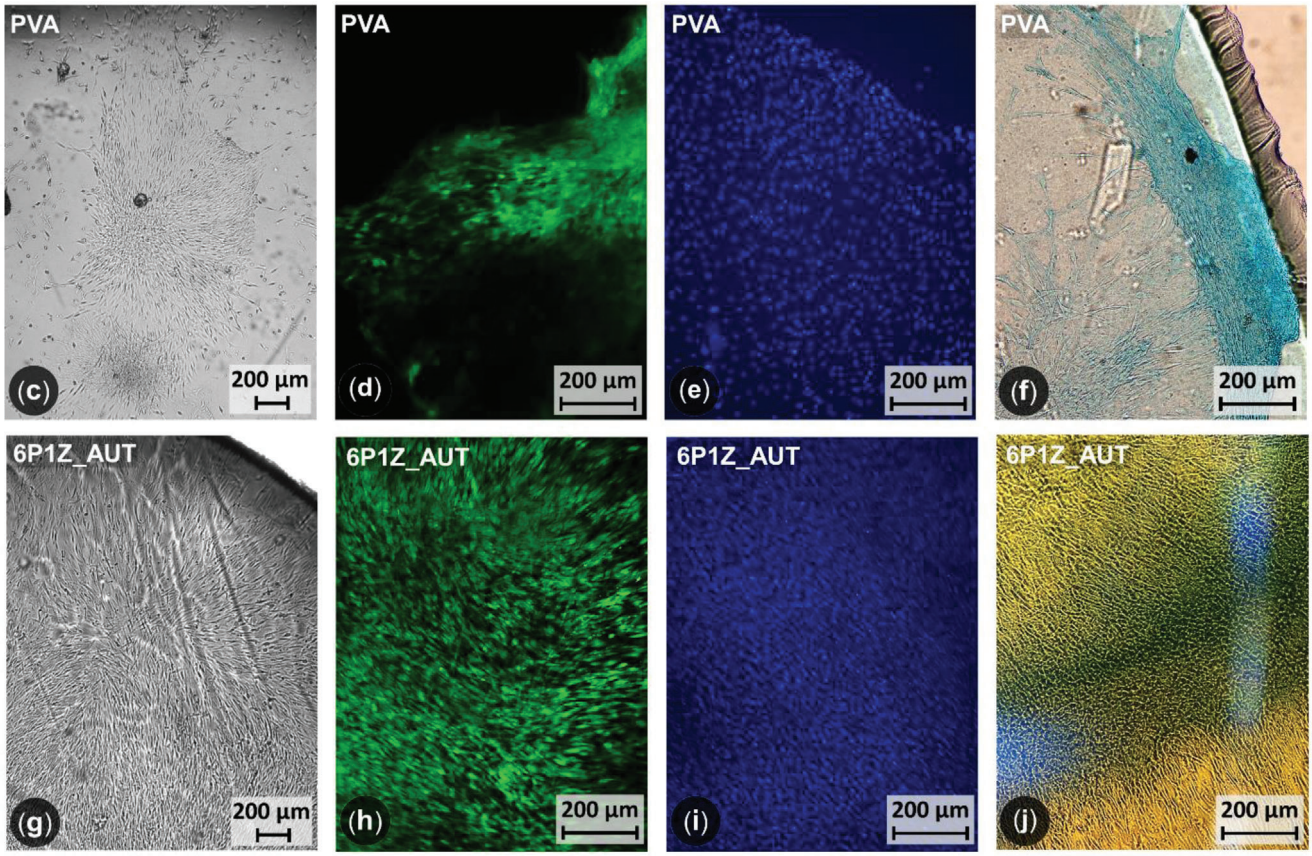

Figure 10. Cellular metabolic activity a) and amount of sulfated glycosaminoglycans per sample b) after chondrocyte culture on the materials for 7 days. The error bars correspond to ± SD. Phase contrast bright-field c,g) and fluorescence images of chondrocytes stained with calcein d,h), DAPI e,i) and Alcian Blue f,j) after cell culture on the materials for 7 days. Metabolic activity data were tested by ANOVA/Tukey's HSD (each type of sample for days 1, 4, or 7) and independent samples *t*-test (PVA vs 6P1Z_AUT for each culture day). The sGAG quantification data were analyzed by independent samples *t*-test. Significant differences ($p < 0.05$) between groups are indicated with an asterisk (*).

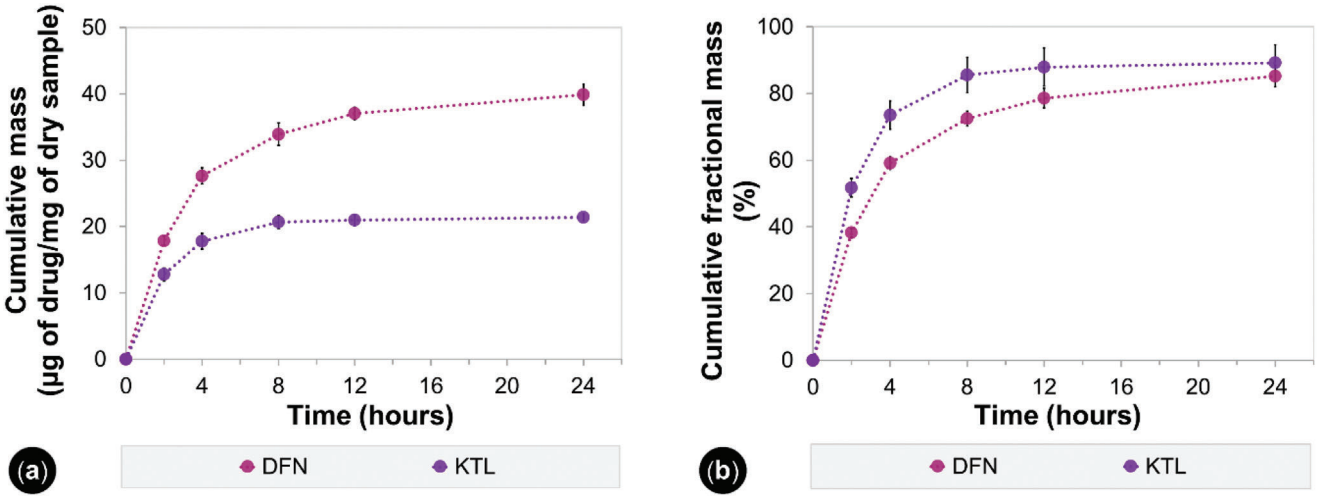

Figure 11. Cumulative DFN and KTL release profiles from 6P1Z_AUT samples, represented in terms of total a) or fractional b) amount of released drugs. The error bars correspond to ± SD.

of reinforcement on the mechanical properties of the water-free composite containing the highest PBO nanofiber content was evaluated by comparison with those of a dry PVA sample (Figure S6 and Table S2 of Supporting Information). The tensile tests revealed that 4.5P1Z far outperforms the unmodified material. The composite could reach values as high as 5019 MPa, 137%, 129 MPa, and 147 MJ m^{-3} for modulus, elongation, strength, and toughness, respectively, which were much higher than those of PVA (1134 MPa, 131%, 39 MPa, and 40 MJ m^{-3}). Although the use of PVA–PBO composites in the dry state is not realistic in the design of cartilage substitutes, they can be useful in other applications where high stiffness, strength, and toughness are of utmost importance. Furthermore, the excellent adhesion between PVA and PBO, a unique feature of this nanofiber-hydrogel composite, solves one of the main problems encountered when designing super-strong fiber-reinforced materials.[42,48,116]

4. Conclusion

In conclusion, PBO nanofibers combined with PVA can form super-strong PVA–PBO composites through a simple gelation process. The new materials were able to reconcile a set of attractive properties such as large water content, high mechanical stiffness, low friction, and excellent biocompatibility, which mimic natural cartilage and are quite difficult to achieve together in other polymeric hydrogels. The PVA–PBO composites could be sterilized by steam heat or gamma radiation without compromising their integrity and overall performance and demonstrated potential for being used as delivery platforms for anti-inflammatory drugs to relieve pain and other inflammatory signals in the postoperative period.

Our findings show that the new engineered PVA–PBO composites have an excellent potential to be used not only in the design of load-bearing tissues, such as articular cartilage, but also in other industrial fields where high thermal stability and mechanical resistance are essential requirements. The feasible tuning of the mechanical properties of these materials based on the nanofiber content, the level of hydration, and possibly the pH of the liquid phase provides them with the advantage of being tailor-made to the specific needs of each application.

Supporting Information

Supporting Information is available from the Wiley Online Library or from the author.

Acknowledgements

This study was financially supported by FCT under grants PD/BD/128140/2016, PTDC/CTM-CTM/29593/2017, PTDC/EME-SIS/0838/2021, UIDB/00100/2020, UIDP/00100/2020, LA/P/0056/2020, UIDB/50022/2020, UIDP/50022/2020, UIDB/04585/2020, UIDB/04565/2020, UIDP/04565/2020, UIDB/04044/2020, UIDP/04044/2020, LA/P/0140/2020, and UIDB/04028/2020. The authors are deeply grateful to Toyobo Co. Ltd. (Osaka, Japan) for offering the Zylon AS fibers. Ricardo Pereira is also thanked for the general technical assistance, kindly provided whenever needed.

Conflict of Interest

The authors declare no conflict of interest.

Data Availability Statement

The data that support the findings of this study are available from the corresponding author upon reasonable request.

Keywords

cartilage replacement, poly(*p*-phenylene-2,6-benzobisoxazole) nanofibers, polyvinyl alcohol hydrogels, super-strong composite materials

Received: June 11, 2022
Revised: October 28, 2022
Published online: December 16, 2022

[1] A. J. Sophia Fox, A. Bedi, S. A. Rodeo, *Sports Health* **2009**, *1*, 461.
[2] D. L. Robinson, M. E. Kersh, N. C. Walsh, D. C. Ackland, R. N. De Steiger, M. G. Pandy, *J. Mech. Behav. Biomed. Mater.* **2016**, *61*, 96.
[3] G. Knutsen, J. O. Drogset, L. Engebretsen, T. R. Gr øntvedt, T. C. Ludvigsen, S. Løken, E. Solheim, T. R. Strand, O. Johansen, *J. Bone Jt. Surg.* **2016**, *98*, 1332.
[4] R. M. Jeuken, P. P. W. Van Hugten, A. K. Roth, U. T. Timur, T. A. E. J. Boymans, L. W. Van Rhijn, W. D. Bugbee, P. J. Emans, *Orthop. J. Sport. Med.* **2021**, *9*, 232596712110312.
[5] S. W. O'Driscoll, *J. Bone Jt. Surg.* **1998**, *80*, 1795.
[6] A. K. Gowd, A. E. Weimer, D. E. Rider, E. C. Beck, A. Agarwalla, L. K. O'Brien, M. J. Alaia, C. M. Ferguson, B. R. Waterman, *Arthrosc. Sport. Med. Rehabil.* **2021**, *3*, e1227.
[7] B. M. Devitt, S. W. Bell, K. E. Webster, J. A. Feller, T. S. Whitehead, *Knee* **2017**, *24*, 508.
[8] K. Walker-Bone, *BMJ* **2000**, *321*, 936.
[9] J. R. Steadman, W. G. Rodkey, J. J. Rodrigo, *Clin. Orthop. Relat. Res.* **2001**, *391*, S362.
[10] F. Yang, J. Zhao, W. J. Koshut, J. Watt, J. C. Riboh, K. Gall, B. J. Wiley, *Adv. Funct. Mater.* **2020**, *30*, 2003451.
[11] L. Xu, X. Zhao, C. Xu, N. A. Kotov, *Adv. Mater.* **2018**, *30*, 1703343.
[12] D. R. King, T. L. Sun, Y. Huang, T. Kurokawa, T. Nonoyama, A. J. Crosby, J. P. Gong, *Mater. Horiz.* **2015**, *2*, 584.
[13] M. Llorens-Gámez, B. Salesa, Á. Serrano-Aroca, *Int. J. Biol. Macromol.* **2020**, *151*, 499.
[14] C. Beddoes, M. Whitehouse, W. Briscoe, B. Su, *Materials* **2016**, *9*, 443.
[15] K. L. Spiller, S. A. Maher, A. M. Lowman, *Tissue Eng. Part B Rev.* **2011**, *17*, 281.
[16] M. Kyomoto, K. Ishihara, in *Materials for Total Joint Arthroplasty: Biotribology of Potential Bearings* (Eds: R. Sonntag, J. P. Kretzer), Imperial College Press, London **2015**, pp. 299–340.
[17] M. C. Cushing, K. S. Anseth, *Science* **2007**, *316*, 1133.
[18] W. Wei, Y. Ma, X. Yao, W. Zhou, X. Wang, C. Li, J. Lin, Q. He, S. Leptihn, H. Ouyang, *Bioact. Mater.* **2021**, *6*, 998.
[19] A. S. Oliveira, O. Seidi, N. Ribeiro, R. R. Colaço, A. P. Serro, *Materials* **2019**, *12*, 3413.
[20] G. K. Tummala, T. Joffre, R. Rojas, C. Persson, A. Mihranyan, *Soft Matter* **2017**, *13*, 3936.
[21] Y.-S. Pan, D.-S. Xiong, R.-Y. Ma, *Wear* **2007**, *262*, 1021.
[22] F. Li, Y. L. Su, D. F. Shi, C. T. Wang, *Adv. Mater. Res.* **2009**, *87–88*, 188.
[23] S. R. Stauffer, N. A. Peppast, *Polymer* **1992**, *33*, 3932.
[24] J. K. Katta, M. Marcolongo, A. Lowman, K. A. Mansmann, *J. Biomed. Mater. Res. Part A* **2007**, *83A*, 471.
[25] C. M. Hassan, N. A. Peppas, in *Biopolymers: PVA Hydrogels, Anionic Polymerisation Nanocomposites*, Advances in Polymer Science, Springer, Berlin **2000**, pp. 37–65.
[26] V. A. Alvarez, J. S. Gonzalez, in *Handbook of Polymer and Ceramic Nanotechnology*, Springer International Publishing, Cham **2021**, pp. 27–37.
[27] A. S. Oliveira, S. Schweizer, P. Nolasco, I. Barahona, J. Saraiva, R. Colaço, A. P. Serro, *Lubricants* **2020**, *8*, 36.
[28] F. V. Sciarretta, *Eur. Rev. Med. Pharmacol. Sci.* **2013**, *17*, 3031.
[29] T. R. Daniels, A. S. E. Younger, M. J. Penner, K. J. Wing, S. L. Miniaci-Coxhead, E. Pinsker, M. Glazebrook, *Foot Ankle Int.* **2017**, *38*, 243.
[30] A. P. Dhand, J. H. Galarraga, J. A. Burdick, *Trends Biotechnol.* **2021**, *39*, 519.
[31] S. Awasthi, J. K. Gaur, S. K. Pandey, M. S. Bobji, C. Srivastava, *ACS Appl. Mater. Interfaces* **2021**, *13*, 24505.
[32] U. G. K. Wegst, H. Bai, E. Saiz, A. P. Tomsia, R. O. Ritchie, *Nat. Mater.* **2015**, *14*, 23.
[33] R. Zhang, Y. Wu, P. Lin, Z. Jia, Y. Zhang, F. Liu, B.o Yu, F. Zhou, *Adv. Eng. Mater.* **2020**, *22*, 2000508.
[34] X. Tong, J. Zheng, Y. Lu, Z. Zhang, H. Cheng, *Mater. Lett.* **2007**, *61*, 1704.
[35] Y. Huang, D. R. King, T. L. Sun, T. Nonoyama, T. Kurokawa, T. Nakajima, J. P. Gong, *Adv. Funct. Mater.* **2017**, *27*, 1605350.
[36] I. Doench, T. Tran, L. David, A. Montembault, E. Viguier, C. Gorzelanny, G. Sudre, T. Cachon, M. Louback-Mohamed, N. Horbelt, C. Peniche-Covas, A. Osorio-Madrazo, *Biomimetics* **2019**, *4*, 19.
[37] C. Zhou, Q. Wu, *Colloids Surf., B* **2011**, *84*, 155.
[38] H. Yao, J. Kang, W. Li, J. Liu, R. Xie, Y. Wang, S. Liu, D.-A. Wang, L.i Ren, *Biomed. Mater.* **2017**, *13*, 015012.
[39] S. Gan, W. Lin, Y. Zou, B. Xu, X. Zhang, J. Zhao, J. Rong, *Carbohydr. Polym.* **2020**, *229*, 115523.
[40] H. Avci, A. Hassanin, T. Hamouda, A. Kiliç, *J. Eng. Archit. Fac. Eskisehir Osmangazi Univ.* **2019**, *27*, 130.
[41] Y. Guan, W. Li, Y. Zhang, Z. Shi, J. Tan, F. Wang, Y. Wang, *Compos. Sci. Technol.* **2017**, *144*, 193.
[42] M. Zboncak, J. Jancar, *eXPRESS Polym. Lett.* **2018**, *12*, 753.
[43] M. Chen, D. Wang, M. Yue, X. Lin, M. Yang, Q. He, *Macromol. Mater. Eng.* **2018**, *303*, 1800229.
[44] A. Serafin, C. Murphy, M. C. Rubio, M. N. Collins, *Mater. Sci. Eng. C* **2021**, *122*, 111927.
[45] Y. Guo, X. An, Z. Fan, *J. Mech. Behav. Biomed. Mater.* **2021**, *118*, 104452.
[46] S. Bourbigot, X. Flambard, F. Poutch, S. Duquesne, *Polym. Degrad. Stab.* **2001**, *74*, 481.
[47] X. Hao, J. Zhu, X. Jiang, H. Wu, J. Qiao, W. Sun, Z. Wang, K. Sun, *Nano Lett.* **2016**, *16*, 2981.
[48] C. Hu, F. Wang, H. Yang, J. Ai, L. Wang, D. Jing, L. Shao, X. Zhou, *J. Dent.* **2014**, *42*, 1560.
[49] A. Rey-Rico, H. Madry, M. Cucchiarini, *Biomed Res. Int.* **2016**, *2016*, 1215263.
[50] A. S. Oliveira, I. Ferreira, A. C. Branco, J. C. Silva, C. Costa, P. Nolasco, A. C. Marques, D. Silva, R. Colaço, C. G. Figueiredo-Pina, A. P. Serro, *J. Biomed. Mater. Res., Part B* **2022**, *110*, 1839.
[51] A. C. Branco, A. S. Oliveira, I. Monteiro, P. Nolasco, D. C. Silva, C. G. Figueiredo-Pina, R. Colaço, A. P. Serro, *Gels* **2022**, *8*, 143.
[52] R. Galante, T. J. A. Pinto, R. Colaço, A. P. Serro, *J. Biomed. Mater. Res., Part B* **2018**, *106*, 2472.
[53] A. Topete, C. A. Pinto, H. Barroso, J. A. Saraiva, I. Barahona, B. Saramago, A. P. Serro, *ACS Biomater. Sci. Eng.* **2020**, *6*, 4051.
[54] W. L. Stoppel, J. C. White, S. D. Horava, A. C. Henry, S. C. Roberts, S. R. Bhatia, *J. Biomed. Mater. Res., Part B* **2014**, *102*, 877.
[55] N. E. George, C. Gurk-Turner, N. S. Mohamed, W. A. Wilkie, E. A. Remily, I. M. D. Castrodad, E. Roadcloud, R. Delanois, *Cureus* **2020**, *12*, e7310.
[56] C.-C. Chen, J.-C. Yang, D.-Y. Ji, Y. Lu, Patent No. US20100003519A1, **2010**.
[57] H. Osatake, T. Inoué, *Arch. Histol. Cytol.* **1988**, *51*, 53.
[58] International Organization for Standardization. ISO 10993-5, *Biological evaluation of medical devices—Part 5: Tests for in vitro cytotoxicity*, **2009**.
[59] J. Nam, J. Johnson, J. J. Lannutti, S. Agarwal, *Acta Biomater.* **2011**, *7*, 1516.
[60] J. C. Silva, C. S. Moura, G. Borrecho, A. P. A. Matos, C. L. Da Silva, J. M. S. Cabral, P. J. Bártolo, R. J. Linhardt, F. C. Ferreira, *Biotechnol. J.* **2020**, *15*, 1900078.
[61] K. Fujii, S. Brownstein, A. M. Eastham, *J. Polym. Sci. Part A-1: Polym. Chem.* **1968**, *6*, 2377.
[62] X.-D. Hu, S. E. Jenkins, B. G. Min, M. B. Polk, S. Kumar, *Macromol. Mater. Eng.* **2003**, *288*, 823.
[63] M. Chen, Y. Mo, Z. Li, X. Lin, Q. He, *Eur. Polym. J.* **2016**, *84*, 622.
[64] M. Pääkkö, M. Ankerfors, H. Kosonen, A. Nykänen, S. Ahola, M. Österberg, J. Ruokolainen, J. Laine, P. T. Larsson, O. Ikkala, T. Lindström, *Biomacromolecules* **2007**, *8*, 1934.

[65] Q. Ma, B. Wang, J. Lv, Y. Li, H. Li, C. Zhao, *Mater. Res. Express* **2017**, *4*, 085301.
[66] K. Tamargo-Martínez, S. Villar-Rodil, J. I. Paredes, A. Martínez-Alonso, J. M. D. Tascón, *Chem. Mater.* **2003**, *15*, 4052.
[67] J. Chin, A. Forster, C. Clerici, L. Sung, M. Oudina, K. Rice, *Polym. Degrad. Stab.* **2007**, *92*, 1234.
[68] Z. Liu, X. Fan, L. Cheng, J. Zhang, L. Tang, Y. Tang, J. Kong, J. Gu, *Adv. Fiber Mater.* **2022**, *4*, 520.
[69] L. Tang, J. Zhang, J. Gu, *Chinese J. Aeronaut* **2021**, *34*, 659.
[70] T. Kitagawa, in *Handbook of Textile Fibre Structure* (Eds: S. J. Eichhorn, J. W. S. Hearle, M. Jaffe, T. Kikutani), Elsevier, Amsterdam **2009**, pp. 429–454.
[71] J. Coates, in *Encycl. Anal. Chem.*, John Wiley & Sons, Ltd, Chichester, UK **2006**.
[72] S. Guzman-Puyol, L. Ceseracciu, J. A. Heredia-Guerrero, G. C. Anyfantis, R. Cingolani, A. Athanassiou, I. S. Bayer, *Chem. Eng. J.* **2015**, *277*, 242.
[73] L. Zhong, S. F. Parker, *R. Soc. Open Sci.* **2018**, *5*, 181363.
[74] S. Sugumaran, C. S. Bellan, *Optik* **2014**, *125*, 5128.
[75] G. A. Holmes, K. Rice, C. R. Snyder, *J. Mater. Sci.* **2006**, *41*, 4105.
[76] C.h. L. Raju, J. L. Rao, B. C. V. Reddy, K. Veera Brahmam, *Bull. Mater. Sci.* **2007**, *30*, 215.
[77] F. Reguieg, L. Ricci, N. Bouyacoub, M. Belbachir, M. Bertoldo, *Polym. Bull.* **2020**, *77*, 929.
[78] M. I. Voronova, O. V. Surov, S. S. Guseinov, V. P. Barannikov, A. G. Zakharov, *Carbohydr. Polym.* **2015**, *130*, 440.
[79] B. J. Holland, J. N. Hay, *Polymer* **2001**, *42*, 6775.
[80] P. Song, Z. Xu, Y. Lu, Q. Guo, *Compos. Sci. Technol.* **2015**, *118*, 16.
[81] M. Ghorbani, L. Roshangar, J. Soleimani Rad, *Eur. Polym. J.* **2020**, *130*, 109697.
[82] R. Brocklehurst, M. T. Bayliss, A. Maroudas, H. L. Coysh, M. A. Freeman, P. A. Revell, S. Y. Ali, *J. Bone Joint Surg. Am.* **1984**, *66*, 95.
[83] E. Jung, H. J. Choi, M. Lim, H. Kang, H. Park, H. Han, B.-H. Min, S. Kim, I. Park, H. Lim, *Biomed. Opt. Express* **2012**, *3*, 1110.
[84] J. A. Hunt, R. Chen, T. Van Veen, N. Bryan, *J. Mater. Chem. B* **2014**, *2*, 5319.
[85] O. Erol, A. Pantula, W. Liu, D. H. Gracias, *Adv. Mater. Technol.* **2019**, *4*, 1900043.
[86] L. Cacopardo, N. Guazzelli, R. Nossa, G. Mattei, A. Ahluwalia, *J. Mech. Behav. Biomed. Mater.* **2019**, *89*, 162.
[87] A. Tamayol, M. Akbari, Y. Zilberman, M. Comotto, E. Lesha, L. Serex, S. Bagherifard, Y. Chen, G. Fu, S. K. Ameri, W. Ruan, E. L. Miller, M. R. Dokmeci, S. Sonkusale, A. Khademhosseini, *Adv. Healthcare Mater.* **2016**, *5*, 711.
[88] Q. Shi, H. Liu, D. Tang, Y. Li, X. Li, F. Xu, *NPG AsiaMater* **2019**, *11*, 64.
[89] A. Richter, G. Paschew, S. Klatt, J. Lienig, K.-F. Arndt, H.-J. Adler, *Sensors* **2008**, *8*, 561.
[90] F. Boschetti, G. M. Peretti, *Biorheology* **2008**, *45*, 337.
[91] M. Charlebois, M. D. Mckee, M. D. Buschmann, *J. Biomech. Eng.* **2004**, *126*, 129.
[92] S. Roberts, B. Weightman, J. Urban, D. Chappell, *J. Bone Joint Surg. Br.* **1986**, *68-B*, 278.
[93] O. Démarteau, L. Pillet, A. Inaebnit, O. Borens, T. M. Quinn, *Osteoarthr. Cartil.* **2006**, *14*, 589.
[94] M. Bartnikowski, R. Wellard, M. Woodruff, T. Klein, *Polymers* **2015**, *7*, 2650.
[95] K. Qiao, Y. Zheng, S. Guo, J. Tan, X. Chen, J. Li, D. Xu, J. Wang, *Compos. Sci. Technol.* **2015**, *118*, 47.
[96] A. Oliveira, *Effects of Sterilization on Drug Loaded Ophthalmic Lenses Materials*, Instituto Superior Técnico–University of Lisbon, Lisbon **2016**.
[97] M. Gilbert, in *Brydson's Plastics Materials*, Elsevier, Amsterdam **2017**, pp. 487–511.
[98] M. Messiha, A. Frank, F. Arbeiter, G. Pinter, *Polymer* **2022**, *239*, 124437.
[99] A. Neville, A. Morina, T. Liskiewicz, Y. Yan, *Proc. Inst. Mech. Eng. Part C: J. Mech. Eng. Sci.* **2007**, *221*, 1223.
[100] H. Hertz, *J. Reine Angew. Math.* **1881**, *92*, 156.
[101] O. R. Schätti, V. Colombo, P. A. Torzilli, L. M. Gallo, *Biorheology* **2018**, *54*, 109.
[102] M. D. Harris, A. E. Anderson, C. R. Henak, B. J. Ellis, C. L. Peters, J. A. Weiss, *J. Orthop. Res.* **2012**, *30*, 1133.
[103] Y. Shi, D. Xiong, J. Li, N. Wang, *RSC Adv.* **2016**, *6*, 82467.
[104] F. Li, Y. Su, J. Wang, G. Wu, C. Wang, *J. Mater. Sci. Mater. Med.* **2010**, *21*, 147.
[105] H. Forster, J. Fisher, *Proc. Inst. Mech. Eng. Part H J. Eng. Med.* **1999**, *213*, 329.
[106] Y. Chen, J. Song, S. Wang, W. Liu, *Macromol. Biosci.* **2021**, *21*, 2100147.
[107] T. Noguchi, T. Yamamuro, M. Oka, P. Kumar, Y. Kotoura, S.-H. Hyonyt, Y. Ikadat, *J. Appl. Biomater.* **1991**, *2*, 101.
[108] W.-Y. Chuang, T.-H. Young, C.-H. Yao, W.-Y. Chiu, *Biomaterials* **1999**, *20*, 1479.
[109] J. C. Silva, X. Han, T. P. Silva, K. Xia, P. E. Mikael, J. M. S. Cabral, F. C. Ferreira, R. J. Linhardt, *Glycoconj. J.* **2020**, *37*, 345.
[110] B. E. Uygun, S. E. Stojsih, H. W. T. Matthew, *Tissue Eng., Part A* **2009**, *15*, 3499.
[111] A. Topete, A. S. Oliveira, A. Fernandes, T. G. Nunes, A. P. Serro, B. Saramago, *Eur. J. Pharm. Sci.* **2018**, *117*, 107.
[112] S. Ghalei, H. Asadi, B. Ghalei, *J. Appl. Polym. Sci.* **2018**, *135*, 46643.
[113] R. Chadha, N. Kashid, D. V. S. Jain, *Pharmazie* **2003**, *58*, 631.
[114] J. Roy, M. Islam, A. H. Khan, S. C. Das, M. Akhteruzzaman, A. K. Deb, A. H. M. Alam, *J. Pharm. Sci.* **2001**, *90*, 541.
[115] A. Topete, B. Saramago, A. P. Serro, *Int. J. Pharm.* **2021**, *602*, 120613.
[116] R. Sa, Y. Yan, Z. Wei, L. Zhang, W. Wang, M. Tian, *ACS Appl. Mater. Interfaces* **2014**, *6*, 21730.